Universität Bremen
Fachbereich 1
Institut für Theoretische Physik

Studienarbeit

Theoretical Description of Superradiance for two-level Emitters in optical Resonators

Simon Müller

Mat. Nr. 213 5901

Bremen, den 13. September 2008

1. Gutachter	Prof. Dr. Frank Jahnke
2. Gutachter	Prof. Dr. Peter Richter
Betreuung	Dr. Paul Gartner

Acknowledgements

I would like to thank Dr. Paul Gartner for great supervision, support and a lot of patience. Prof. Frank Jahnke for giving me an interesting and fruitful topic and great supervision, as well. Christopher Gies for understanding what it is like to write a Studienarbeit and saying the right things at the right time. In addition my thank goes to Sandra Ritter and Michael Lorke for their help.

Contents

Chapter 1

Introduction

The interaction between light and matter gives rise to a great number of physical phenomena with multitudinous applications. One form of this interaction, the emission and absorption of light, is caused by a change of the quantum-mechanical state of an electrically charged material system. A prominent example is the radiation emitted and absorbed by an electron bound by the electric potential of an atomic nucleus. Recently, different types of systems, so called quantum dots (QDs) (12), have become the focus of a large amount of research effort.

A QD is a semiconductur structure, spatially confining a small number of carriers. The volume edge lengths are the order of the *de Broglie* wavelength of the enclosed electrons. Therefore the system can be viewed as being zero dimensional. As a consequence of spatial confinement, the spectrum of the enclosed carriers is discrete. The energy levels can be manipulated by choice of material, confinement potential and geometry (15) of the QDs, making possible emission of radiation in a wide spectral range.

An established method is the Stranski-Krastanov growth of QDs (16), which is based on strain-induced island formation of a material on a substrate, both materials slightly varying in their lattice constant. Samples obtained in this way have densities of the order $10^9 - 10^{10}\ \frac{\text{QDs}}{\text{cm}^2}$ and exhibit a spectral inhomogeneous broadening due to fluctuations in size and composition.

The theory of the current work rests in the framework of the *Jaynes–Cummings* model, presented in section 2.2. QDs are treated as two-level systems[1] all exposed to the same electro-magnetic field. The field is incorpo-

[1] It is known that QDs behave differently than two-level systems (3). Yet, this assumption is often made in order to have a straight-forward theoretical description.

rated as a single, quantized resonator mode. The quantization is described in section 2.1. The the light matter interaction is included in dipole and rotating wave approximation (see section 2.2 for details). Dissipative processes are included in *Born-Markov* approximation in section 2.4. The density matrix formalism is briefly described in 2.3.

Interaction effects between a set of radiating QDs are the object of current research and the focus of this work. The *spontaneous* emission of several QDs, interacting with a single-mode electric field is studied. Under certain conditions, coupling between several QDs leads to *superradiance*. The term refers to a non-linear enhancement of the maximum radiation. The first theoretical account of the effect was given by Dicke in 1954 (5). He describes N identical emitters, all exposed to an identical electro-magnetic field and gives a theoretical account for spontaneous emission for this setup. What he shows is that, under certain conditions, the maximum intensity of radiation does not scale linearly with the number of emitters but quadratically. Dickes treatment deals with the spontaneous emission of number of gas molecules confined to a small volume[2] (5). The theory was originally developed to understand effects of radiation in the MHz region. Today, superradiance may provide the basis for enhancement and manipulation of emission processes in the optical region. Although theoretical work has been carried out (14), it is an open question, whether superradiant effects play an important role in the behavior of a set of closely spaced QDs. In order to address this question, a theoretical model for a set of quantum dots jointly emitting radiation is presented, and its physical implications are explored by numerical solution of the corresponding *von Neumann* equation.

The obtained results are presented in chapter 3. Numerical accuracy is assessed by comparison with analytical results for one and two atoms. Those density matrix entries giving rise to superradiance are identified. When cavity losses are in the order of $\kappa = 1.5\frac{1}{ps}$ and superradiance is suppressed, effects attributed to stimulated emission and absorption are observed. Superradiant emission for a set of emitters for different initial conditions is characterized. The results of solving the full density matrix with dissipation are compared to a master equation approach (1). The results show differences in the early

[2]Small means that the wavelength of the emitted radiation is orders of magnitude greater than the edge lengths of the volume.

phases of the superradiant pulse. The master equation is found to overestimate superradiant contributions. Finally, the effect of inhomogeneous broadening is presented for a set of $N = 5$ emitters. The effect is found to be robust to detunings in the order of $0.5 - 1.0meV$ with a coupling strength of $g = 0.2\frac{1}{ps}$ and a cavity loss constant of $\kappa = 1.5\frac{1}{ps}$. The biexponential decay reported in (14) is reproduced for these parameters.

Chapter 2

Theoretical model

The theoretical framework of the current work is provided by two main components. The first one is the *Jaynes–Cummings* model of light–matter interaction. It combines a simple two-level approach to model the matter sub–system (referred to as atomic system), and a quantized, single–mode electro–magnetic field. The second component is dissipation. It is important to arrive at system dynamics which are not only oscillations . Dissipation enters the theoretical description in second order of the interaction (*Born* approximation). In addition, memory effects are neglected (*Markov* approximation). The components of the model are first presented and then combined at the end of the chapter.

2.1 Field quantization

In the study of physical systems involving electro-magnetism, a fully quantized treatment of the electro-magnetic field is usually avoided, since the quantization can be accompanied by some difficulties. In addition, most phenomena can be understood very well in models with the light field treated classically. The hydrogen problem might be the most prominent example for this, since the electro-static potential enters the Hamiltonian as a continuous, scalar function.

As Allen and Eberly point out in (2), there are some few cases where a fully quantized description provides either better insight into the system dynamics, or phenomena can only be understood, if the field is treated as a quantum system. An example of the first case is the *Jaynes-Cummings* model (9). Spontaneous emission falls into the latter category, since atoms radiate

spontaneously even if the electro-magnetic field is in the vacuum state – a process that can not be understood in classical terms. The following account of field quantization follows (11) and is limited to the quantization within a finite volume.

2.1.1 Single-mode field quantization

We first study the quantization of a single-mode electro-magnetic field. The mode is assumed to be restricted to a cubic cavity with volume V and edge lengths $V_x = V_y = V_z$. We proceed in the following manner: first an expression for the *classical* field Hamiltonian is derived. Then this is identified as the Hamiltonian of an harmonic oscillator, making it possible to treat the quantization in full analogy.

The field mode is assumed to be constant along the x- and y-dimension. Its polarization vector $\mathbf{p} = (1, 0, 0)$ points in the x-direction. This can be expressed as

$$\mathbf{E}(z, t) = \mathbf{p} A(t) \sqrt{\frac{2\Omega^2}{\varepsilon_0 V}} \sin(Kz), \tag{2.1}$$

where $A(t)$ is the time-dependent field amplitude oscillating at the frequency Ω. ε_0 is the free space permittivity and $\mathbf{K} = (0, 0, K)$ the wave-number, with

$$\sin(KV_z) = 0.$$

The normalization $\sqrt{\frac{2\Omega^2}{\varepsilon_0 V}}$ will turn out to be a good choice, when transforming the Hamiltonian.

Since the magnetic field $\mathbf{B}$ contributes to the field energy as well, we must find an expression for $\mathbf{B}$ in order to be able to express the field Hamiltonian.

Applying the wave-equation

$$\Delta \mathbf{E} = \frac{1}{c^2} \frac{\partial^2 \mathbf{E}}{\partial t^2}, \tag{2.2}$$

where c is the vacuum speed of light, to the electric field (2.1) yields

$$-K^2 \mathbf{E} = \frac{1}{c^2} \ddot{A}(t) \frac{\mathbf{E}}{A}.$$

From this we can derive an equation for $A(t)$.

$$A(t) = -\frac{1}{K^2c^2}\ddot{A}(t) \tag{2.3}$$

In addition, applying the the *Maxwell* equation

$$\nabla \times \mathbf{E} = -\frac{\partial \mathbf{B}}{\partial t} \tag{2.4}$$

to the electric field (2.1) we can derive the time derivative of $\mathbf{B}$

$$-\frac{\partial \mathbf{B}}{\partial t} = \mathbf{p}' A(t)\sqrt{\frac{2\Omega^2}{\varepsilon_0 V}}K\cos(Kz), \tag{2.5}$$

with $\mathbf{p}' = (0,1,0)$. By substituting the equation for the field amplitude $A(t)$ (2.3) into the time derivative of $\mathbf{B}(t)$ (2.5) we can find an easily integrated equation for $\mathbf{B}$.

$$-\frac{\partial \mathbf{B}}{\partial t} = -\frac{1}{K^2c^2}\mathbf{p}'\ddot{A}(t)\sqrt{\frac{2\Omega^2}{\varepsilon_0 V}}K\cos(Kz) \tag{2.6}$$

$$\Rightarrow \quad \mathbf{B} = \frac{1}{Kc^2}\mathbf{p}'\dot{A}(t)\sqrt{\frac{2\Omega^2}{\varepsilon_0 V}}\cos(Kz). \tag{2.7}$$

Now we have all the components needed for the field Hamiltonian. The overall energy of the field is found by integrating the energy density $\mathscr{U}$ over the entire resonator volume: The classical Hamiltonian of the electromagnetic field is

$$H = \int_V \mathscr{U}\, dV = \frac{1}{2}\int_V \varepsilon_0 E^2 + \frac{1}{\mu_0}B^2\, d^3r. \tag{2.8}$$

Inserting the expressions found for $\mathbf{E}$ and $\mathbf{B}$ this gives

$$H = \frac{\Omega^2}{V}\int_V A^2(t)\sin^2(Kz) + \frac{1}{K^2c^2}\dot{A}^2(t)\cos^2(Kz)\, d^3r \tag{2.9}$$

$$= \frac{\Omega^2}{V^{1/3}}\left(A^2(t)\cdot\left[\frac{V^{1/3}}{2} - \frac{\sin(2KV_z)}{4K}\right]\right) + \frac{1}{V^{1/3}}\left(\dot{A}^2(t)\left[\frac{V^{1/3}}{2} + \frac{\sin(2KV_z)}{4K}\right]\right) \tag{2.10}$$

$$= \frac{\Omega^2}{2}\left(A^2(t) + \frac{1}{\Omega^2}\dot{A}^2(t)\right). \tag{2.11}$$

Assigning $A = q$ and $\dot{A} = p$ the analogy to the harmonic oscillator becomes evident[1].

Defining the so called annihilation operator $b = \frac{1}{\sqrt{2\Omega\hbar}}(\Omega q + ip)$ and its adjoint, the creation operator $b = \frac{1}{\sqrt{2\Omega\hbar}}(\Omega q - ip)$, we can write for the Hamiltonian

$$H = \hbar\Omega(b^\dagger b + \tfrac{1}{2}). \tag{2.12}$$

The difference between the harmonic oscillator and the field Hamiltonian (2.12) lies in the interpretation of the different eigenstates of the Hamiltonian. In the field case it is the possible field modes that have quantized energies, as compared to the levels of excitation of a single oscillator. The eigenstates $|n\rangle$ of the Hamiltonian (2.12) are states with a defined *photon* number:

$$H|n\rangle = \hbar\Omega(n + \tfrac{1}{2})|n\rangle, \qquad n = 0, 1, 2 \ldots. \tag{2.13}$$

Expressing the operator A in terms of b and $b^\dagger$ gives $A = \sqrt{\hbar/2\Omega}(b + b^\dagger)$. We therefore have

$$E = \mathscr{E}_\Omega(b + b^\dagger)\sin(Kz) \tag{2.14}$$

as the electric field operator, the quantum mechanical version of the electric field (2.1), with the constant $\mathscr{E}_\Omega = \sqrt{\frac{\hbar\Omega}{\varepsilon_0 V}}$.

2.1.2 Multi-mode field quantization

As a direct consequence of the superposition principle, that holds for fields satisfying *Maxwell's* equations, the multi-mode Hamiltonian is the sum of the contributing single-mode Hamiltonians:

$$H = \sum_k H_k = \hbar \sum_k \Omega_k(b_k^\dagger b_k + \tfrac{1}{2}), \tag{2.15}$$

where k indexes all wave-numbers and possible polarisations. The same is true for the field operator (2.14) which in our case is

$$E = \sum_k \mathscr{E}_{\Omega_k}(b_k + b_k^\dagger)\sin(kz). \tag{2.16}$$

[1] For an account of the harmonic oscillator, see, e.g., (13) pp. 180.

2.1.3 Coherent states

It can be shown that, for a given field mode k, the eigenstates of the annihilation operator b_k satisfy certain conditions making them *coherent* (7). The dynamics, that the field will be subject to in the following chapters, can be analytically analyzed, if the photon field is in a coherent state. Therefore they will be briefly introduced here. The eigenstates to the annihilation operator are:

$$b|\lambda\rangle = \lambda_\lambda|\lambda\rangle.$$

The states $|\lambda\rangle$ may be generated from a basis of Hamiltonian eigenstates $\{|n\rangle\}as$[2]

$$|\lambda\rangle = e^{-|\lambda|^2/2}\sum_n \frac{\lambda^n}{\sqrt{n}}|n\rangle \tag{2.17}$$

The probability of finding n photons in the state $|\lambda\rangle$ is given by

$$p_n = |\langle n|\lambda\rangle|^2 = e^{-|\lambda|^2}\frac{|\lambda|^{2n}}{n!}. \tag{2.18}$$

This is know as a *Poisson* distribution. This type of probability distribution is characteristic for coherent states of the photon field.

We will now turn to introduce the *Jaynes Cummings* model of light-matter interaction, providing the main theoretical reference frame of the current work.

2.2 The Jaynes-Cummings Hamiltonian

In order to study the interaction between matter and light one must find a model for both, the light and matter systems, and the interaction between them. We have already found the Hamiltonian for the quantum mechanical description of a single-mode light field. What we are still missing are the two

[2]This can be seen by expanding $|\lambda\rangle$ into $|n\rangle$

$$|\lambda\rangle = \sum_n |n\rangle\langle n|\lambda\rangle = \sum_n |n\rangle\langle 0|\lambda^n\sqrt{n!}^{-1}|\lambda\rangle = \langle 0|\lambda\rangle\sum_n \frac{\lambda^n}{\sqrt{n!}}|n\rangle$$

and evaluating $\langle 0|\lambda\rangle$ with proper normalization.

latter model components. We will give a brief account of both in this chapter. The model for the matter system, or atomic system as it will be referred to from here, is chosen to be a simple two-level system. Either one or a set of N identical two-level systems enter the final Hamiltonian. The interaction with the light field will be incorporated in the so called dipole and rotating wave approximations that are explained below. This makes it possible to find the matrix representation of the interaction operator very easily. Taking these three components together we arrive at the *Jaynes-Cummings* model for light-matter interaction.

2.2.1 Light-matter coupling in dipole approximation

The Hamiltonian of a particle interacting with an electro-magnetic field in SI units is given by:

$$H = \frac{1}{2\,m}[\mathbf{p}(t) - e\mathbf{A}(\mathbf{r},t)]^2 + e\Phi(\mathbf{r},t) \tag{2.19}$$

Here, $\mathbf{A}$ is the vector potential of the electro-magnetic field, e is the elementary charge and Φ the scalar electro-static potential. The fields $\mathbf{E}$ and $\mathbf{B}$ are related to the potentials by:

$$\mathbf{E} = -\nabla\Phi - \frac{\partial}{\partial\,t}\mathbf{A} \tag{2.20}$$

$$\mathbf{B} = \nabla \times \mathbf{A}. \tag{2.21}$$

The tool to arrive at the dipole approximation, making the interaction linear in e, is a proper gauge transform ((8),(13)). It makes use of an additional freedom in the theory making it possible to change the potentials, without changing the physical content of the theory. In *Hilbert* space the transformation is given by a unitary transformation T:

$$T = e^{i\frac{e}{\hbar}\chi} \qquad T^{-1} = T^{\dagger}, \tag{2.22}$$

where χ is an arbitrary scalar function. All state vectors and operators must then be transformed according to:

$$|\Psi'\rangle = T\,|\Psi\rangle, \tag{2.23}$$

$$O' = TOT^{-1}. \tag{2.24}$$

It can be shown that the *Schrödinger* equation is satisfied by the new Hamiltonian H':

$$H' = T H T^{-1} - i\hbar T \frac{\partial T^{-1}}{\partial t}, \tag{2.25}$$

We will now try to find a transform that makes the Hamiltonian linear in the interaction.

It will turn out that

$$\chi = -\mathbf{r} \cdot \mathbf{A}$$

is a good choice when applying it to the Hamiltonian (2.19). Note that transformation T commutes with the vector potential $\mathbf{A}$. The effect on the impuls operator $\mathbf{p}$ is:

$$\mathbf{p}' = T(-i\hbar)\frac{\partial}{\partial \mathbf{r}} T^{-1} + T T^{-1} \frac{\partial}{\partial \mathbf{r}} \tag{2.26}$$

$$= e\mathbf{A} + \mathbf{r} \cdot \frac{\partial}{\partial \mathbf{r}} \mathbf{A}(\mathbf{r}, t) + \mathbf{p} \tag{2.27}$$

The typical length scales of the atomic system are 10^{-10}m. The typical radiation wavelengths are in the order of $5 \cdot 10^{-7}$m. The spatial variation of the electro-magnetic field will therefore not be experienced by the atomic system. So when only the interaction with the atomic system is relevant, only negligible errors will be introduced by assuming *almost* spatially constant fields. This implies a spatially constant vector potential $\mathbf{A}$ in the proximity of the atomic system on an atomic length scale. We therefore neglect the middle term in (2.27) and set $\mathbf{A}(\mathbf{r}, t) = \mathbf{A}(0, t)$. This is also known as the dipole approximation.

The second term in the equation (2.25) for the transformation of the Hamiltonian gives:

$$i\hbar T \frac{\partial T^{-1}}{\partial t} = -e\mathbf{r} \cdot \frac{\partial}{\partial t} \mathbf{A} \tag{2.28}$$

$$= e\mathbf{r} \cdot \mathbf{E}, \tag{2.29}$$

given that $\Phi = 0$, as can be seen from equation (2.20) that links the electric field $\mathbf{E}$ to the potentials Φ and $\mathbf{A}$. Setting $\mathbf{d} := e\mathbf{r}$ the new Hamiltonian is then given by:

$$H = \frac{1}{2m}\mathbf{p}^2 + u(\mathbf{r}) - \mathbf{d} \cdot \mathbf{E}. \tag{2.30}$$

Now it can be seen where the name for the approximation comes from. In a classical picture the interaction is that of a dipole with an electric field.

2.2.2 The two-level atom

In many cases, treating an atom as a two-level system is a good approximation that greatly simplifies the analysis of the system. Two of the atomic states are selected and only transitions between these two states are considered. Especially, if the transition energy between two states corresponds to the frequency of a field mode that the atom interacts with, the two-level approach is a good approximation.

The standard description of a two-level quantum-mechanical system is given by the *Pauli* spin-operators. Choosing the z-axis for quantization the corresponding Hamiltonian reads:

$$H = \hbar\tfrac{\omega}{2}\sigma_z. \tag{2.31}$$

The energy difference between the two system states is $E_1 - E_2 = \hbar\omega$. We will refer to the state with higher energy as $|\alpha\rangle$ and the one with lower energy as $|\beta\rangle$.

Together with the identity operator, the raising and the lowering operators σ_+ and σ_- a basis for the associated operator space is given, i.e., any arbitary operator acting on the two-level *Hilbert* sub-space can be expressed as a linear combination of these four operators. Their matrix representation is:

$$\sigma_z = \begin{pmatrix} 1 & 0 \\ 0 & -1 \end{pmatrix} \tag{2.32}$$

$$\sigma_+ = \begin{pmatrix} 0 & 1 \\ 0 & 0 \end{pmatrix} \tag{2.33}$$

$$\sigma_- = \begin{pmatrix} 0 & 0 \\ 1 & 0 \end{pmatrix} \tag{2.34}$$

In particular the dipole operator $\mathbf{d}$ must be expressible as such a linear combination. At this point it is necessary to specify some of the properties of the wave-functions of the two atomic states under consideration. If the

potential entering the atomic Hamiltonian is inversion symmetric, the wavefunctions will have defined parity. This immediately implies that the matrix-representation of $\mathbf{d}$ can only contain off-diagonal entries and that these are related by complex conjugation.[3] So the operator matrix is

$$\mathbf{d} = \begin{pmatrix} 0 & \mathscr{D} \\ \mathscr{D}^* & 0 \end{pmatrix} = \mathscr{D}^* \sigma_- + \mathscr{D} \sigma_+, \tag{2.35}$$

where $\mathscr{D}$ is the dipole-matrix element between the two states.

2.2.3 Rotating wave approximation

We now have all elements needed for a model of light-matter interaction. The atomic system is described by the two-level Hamiltonian (2.31), the field Hamiltonian is (2.12) and the interaction is given in dipole approximation as in (2.30). Using the field operator (2.16) and expressing the dipole operator in terms of σ_- and σ_+, we can write the full Hamiltonian of the coupled light-matter system:

$$H = H_A + H_F + H_I = \hbar\omega\sigma_z + \hbar\Omega b^\dagger b + \hbar(b + b^\dagger)(g\sigma_+ + g^*\sigma_-), \tag{2.36}$$

introducing the light-matter coupling constant

$$g = -\frac{\mathscr{D}\,\mathscr{E}_\Omega}{\hbar} \sin Kz.$$

H_I contains contributions of two distinct types. Multiplying the bracketed terms yields the following combinations: $b\sigma_+$, $b^\dagger\sigma_-$, $b^\dagger\sigma_+$ and $b\sigma_-$. We interpret these contributions as the creation/annihilation of a photon and the transition between the two atomic states.

Near resonance, it is plausible to assume that the dominant contribution is due to the absorption of a photon by the atomic system accompanied by the excitation of the latter or the emission of a photon with the atomic system relaxing from the excited to the ground state. In terms of operators

[3] For two wave functions u_n, u_m the matrix element is given by $\mathbf{d}_{n,m} = e \int u_n^* \, \mathbf{r} \, u_m \, d^3r$. Since the integrand is symmetric only for combinations of n,m corresponding to states with different parity, the assertion follows. Also it can be seen that $d^*_{n,m} = d_{m,n}$ holds by complex conjugation of the integrand and noting that $\mathbf{r}$ is a real operator.

the products $b\sigma_+$ and $b^\dagger\sigma_-$ represent such processes. On the other hand, it appears very unlikely that the generation of a photon is accompanied by the excitation of the atom or the absorption of a photon by the relaxation of the atom. The corresponding operators are $b^\dagger\sigma_+$ and $b\sigma_-$.

Keeping only the two operators discussed first, we arrive at the Hamiltonian in rotating wave approximation (RWA):

$$H_{JC} = \hbar\tfrac{\omega}{2}\sigma_z + \hbar\Omega b^\dagger b + \hbar(gb\sigma_+ + g^* b^\dagger\sigma_-) \tag{2.37}$$

The Hamiltonian (2.37) is known as the *Jaynes-Cummings (JC)* Hamiltonian for a one-atom system. It is amenable to an analytical treatment and some of its properties are to be studied in the following paragraphs.

2.2.4 Analytical treatment of the one-atom Jaynes-Cummings Hamiltonian

The analytic solution of the *Jaynes–Cummings* Hamiltoian (2.37) will be discussed next. After introducing the eigenbasis of the system an remarkable effect observed in the system, so called *Rabi* oscillations, are presented.

Dressed states

Due to the interaction, the eigenstates of the *JC* system do not factorize into eigenstates of the atomic and field Hamiltonians. The new states can be found analytically. After doing so, we will express these states in terms of the field and atomic system states of the non-interacting system to gain some insight into the system dynamics.

Given that the field is in a certain photonic state $|n\rangle$, the dynamics induced by the *JC* Hamiltonian (2.37) connects this state only to one of two other photonic states. If the initial state of the atomic system is $|\alpha\rangle$, then only the field state $|n+1\rangle$ is coupled to $|n\rangle$. In the case of $|\beta\rangle$ for the atomic system, this is $|n-1\rangle$.

This makes H block-diagonal if the basis is chosen as $\{|\alpha\ n\rangle, |\beta\ n+1\rangle\}$:

$$H = \bigoplus_{n=0}^{\infty} H_n. \tag{2.38}$$

In addition, we may chose the dipole-matrix elements between the two atomic states to be real, since we can always find an appropriate choice of phase for the atomic wave-functions. As a matrix H_n has the form:

$$H_n = \hbar \begin{pmatrix} \Omega n + \frac{1}{2}\omega & g\sqrt{n+1} \\ g\sqrt{n+1} & \Omega n - \frac{1}{2}\omega \end{pmatrix} \tag{2.39}$$

$$= \hbar\Omega(n+1/2)\begin{pmatrix} 1 & 0 \\ 0 & 1 \end{pmatrix} + \frac{\hbar}{2}\begin{pmatrix} \delta & 2g\sqrt{n+1} \\ 2g\sqrt{n+1} & -\delta \end{pmatrix} \tag{2.40}$$

Since H_n is symmetric, it can be diagonalized. The resulting eigenstates are referred to as *dressed states*[4]. The (orthogonal) diagonalization transformation is given by:

$$R = \begin{pmatrix} \cos\theta_n & -\sin\theta_n \\ \sin\theta_n & \cos\theta_n \end{pmatrix}, \tag{2.41}$$

with

$$\cos\theta_n = \frac{\mathscr{R}_n - \delta}{\sqrt{(\mathscr{R}_n - \delta)^2 + 4g^2(n+1)}}, \tag{2.42}$$

$$\sin\theta_n = \frac{2g\sqrt{n+1}}{\sqrt{(\mathscr{R}_n - \delta)^2 + 4g^2(n+1)}}, \tag{2.43}$$

$$\mathscr{R}_n = \sqrt{\delta^2 + 4g^2(n+1)}. \tag{2.44}$$

$\delta = \omega - \Omega$ is the detuning between the atomic system and the field mode. The dressed states and their energies are:

$$|2\ n\rangle = \cos\theta_n\,|\alpha\ n\rangle - \sin\theta_n\,|\beta\ n+1\rangle, \tag{2.45}$$

$$|1\ n\rangle = \sin\theta_n\,|\alpha\ n\rangle + \cos\theta_n\,|\beta\ n+1\rangle, \tag{2.46}$$

$$E_{2n} = \hbar(\Omega n - \tfrac{1}{2}\mathscr{R}_n), \tag{2.47}$$

$$E_{1n} = \hbar(\Omega n + \tfrac{1}{2}\mathscr{R}_n). \tag{2.48}$$

Rabi-oscillations

As can be seen from the sub-matrix H_n (2.40), H_n can be split up into a part that is merely a multiple of the identity matrix – and thus not influenced by

[4]The following results are taken from *Maystre Sargent*, (11)

the transformation R – and a second part, that is transformed under R. It is therefore possible to first go into an interaction picture absorbing the time dependence due to the first term $U(t) = \exp -i(n + 1/2)\Omega$, and later apply R.

In this interaction picture the time evolution of the coefficients of a state $|\Psi\rangle$ with

$$|\Psi\rangle = C_{2n}(t)\,|2n\rangle + C_{1n}(t)\,|1n\rangle$$

is given by

$$\begin{pmatrix} C_{2n}(t) \\ C_{1n}(t) \end{pmatrix} = \begin{pmatrix} \exp \frac{1}{2} i\mathscr{R}_n\, t & 0 \\ 0 & \exp -\frac{1}{2} i\mathscr{R}_n\, t \end{pmatrix} \begin{pmatrix} C_{2n}(0) \\ C_{1n}(0) \end{pmatrix}.$$

Transforming back into the non-dressed basis yields

$$\begin{pmatrix} C_{\alpha n}(t) \\ C_{\beta n+1}(t) \end{pmatrix} = \begin{pmatrix} a & b \\ b & a^* \end{pmatrix} \begin{pmatrix} C_{\alpha n}(0) \\ C_{\beta n+1}(0) \end{pmatrix}, \tag{2.49}$$

where

$$a = \cos(\tfrac{1}{2}\mathscr{R}_n t) - i\delta\mathscr{R}_n^{-1} \sin(\tfrac{1}{2}\mathscr{R}_n t), \tag{2.50}$$
$$b = -2ig\sqrt{n+1}\mathscr{R}_n^{-1} \sin(\tfrac{1}{2}\mathscr{R}_n t).$$

For the resonant case with an initially excited atom this simplifies to

$$|C_{\alpha n}(t)|^2 = \cos^2(g\sqrt{n+1}t), \tag{2.51}$$

$$|C_{\beta n+1}(t)|^2 = \sin^2(g\sqrt{n+1}t). \tag{2.52}$$

This behavior is know as *Rabi*-flopping or *Rabi*-oscillation. The eigenstates of the single atom *JC* Hamiltonian are a coherent superposition of the eigenstates of the non-interacting light-matter system. The coefficients of this superposition show an oscillatory behavior as a function of time. One may interpret this physically as the emission of a photon by the atom into the field and the reabsorption of the photon at a later time.

When the modulus of the detuning $|\delta| \neq 0$, the oscillation frequency increases while the amplitude decreases monotonously with the modulus of the detunig $|\delta|$, as can be seen from the factor in front of the sine-function in (2.50)[5] .

[5] If the system is initially in the excited state $|\alpha\rangle$ or in the ground state $|\beta\rangle$ the occupation probability of the initial state as a function of time is $|a|^2$. If the detuning is zero, the squared modulus is zero whenever the cos-function in (2.50) is. The lower bound of $|a|^2$ increases with increasing $|\delta|$, since $\delta\,\mathscr{R}_1$ increases.

2.2.5 The N-atom Jaynes-Cummings Hamiltonian

A *Jaynes-Cummings* system can be expanded to include more than one two-level system. If it is reasonable to assume that all atomic systems experience the photon field at the same location and when there is no direct interaction between the different atomic systems, the multi-atom Hamiltonian for N atoms is

$$H = \sum_n^N \hbar\tfrac{\omega_n}{2}\sigma_{z,n} + \hbar\Omega b^\dagger b + \hbar\sum_n^N (gb\sigma_{+,n} + g^* b^\dagger \sigma_{-,n}) \tag{2.53}$$

$$= \hbar\tfrac{\omega}{2}\Sigma_z + \hbar\Omega b^\dagger b + \hbar(gb\Sigma_+ + g^* b^\dagger \Sigma_-). \tag{2.54}$$

In the last line we have introduced the total spin operators $\Sigma_i = \sum_n^N \sigma_{i,n}$. They obey the same commutation relations as the single-atom operators. In addition, we have set all atoms to have the same transition energy ω between the two states. This condition must be relaxed to account for inhomogeneous broadening, an effect present when the matter system consists of a number of QDs. The respective Hamiltonian is

$$H = \hbar\sum_{i=1}^N \omega_i\sigma_{z,i} + \hbar\Omega b^\dagger b + \hbar(gb\Sigma_+ + g^* b^\dagger \Sigma_-). \tag{2.55}$$

Although there is no direct interaction between the atoms, there are significant cooperative effects that cause the multi-atom system to be more than the sum of its single-atom parts. This is due to the interaction of all atomic systems with the same field mode. One such effect is know as *supperradiance*. This feature of the multi-atom case is discussed in chapter (2.6).

We will next turn to solving the multi-atom problem for $N = 2$ and $\omega = \Omega$. This will give a first insight into the behavior of a multi-atom *Jaynes-Cummings* system and provide an additional basis for comparison with the algorithm implementation.

2.2.6 Analytical treatment of the two atom Jaynes-Cummings Hamiltonian

In the case of two identical atoms and a real-valued coupling constant g, the N-atom *JC* Hamiltonian simplifies to:

$$H = \hbar\tfrac{\omega}{2}(\sigma_{z,1} + \sigma_{z,2}) + \hbar\Omega b^\dagger b + \hbar g\, b(\sigma_{+,1} + \sigma_{+,2}) + \hbar b^\dagger\, g(\sigma_{-,1} + \sigma_{-,2}). \tag{2.56}$$

As in the one-atom case, H can be written in a block-diagonal form. The only complication is that now the the basis of the atomic states has four elements. For a given index value n[6] , we chose the following basis:

$$\{|\alpha,\alpha,n\rangle,\ |\alpha,\beta,n+1\rangle,\ |\beta,\alpha,n+1\rangle,\ |\beta,\beta,n+2\rangle\}\,.$$

The corresponding block H_n is then:

$$H_n = \hbar\Omega(n+1)\begin{pmatrix} 1 & 0 & 0 & 0 \\ 0 & 1 & 0 & 0 \\ 0 & 0 & 1 & 0 \\ 0 & 0 & 0 & 1 \end{pmatrix} \tag{2.57}$$

$$+\hbar\begin{pmatrix} \delta & g\sqrt{n+1} & g\sqrt{n+1} & 0 \\ g\sqrt{n+1} & 0 & 0 & g\sqrt{n+2} \\ g\sqrt{n+1} & 0 & 0 & g\sqrt{n+2} \\ 0 & g\sqrt{n+2} & g\sqrt{n+2} & -\delta \end{pmatrix}. \tag{2.58}$$

In the resonant case ($\delta = 0$), H_n can be diagonalized by the following transformation:

$$T = \begin{pmatrix} -a^{-1} & a & 0 & a \\ 0 & -b & -1 & b \\ 0 & -b & 1 & b \\ 1 & 1 & 0 & 1 \end{pmatrix}, \tag{2.59}$$

with

$$a = \frac{\sqrt{n+1}}{\sqrt{n+2}}, \quad b = -\frac{\sqrt{3+2n}}{\sqrt{2(n+2)}}.$$

The new eigenvalues are given by

$$\begin{aligned} E_0 &= \hbar\Omega(n+1) \\ E_{1,+1} &= \hbar\Omega(n+1) + \sqrt{2g^2(3+2n)} \\ E_{1,0} &= \hbar\Omega(n+1) \\ E_{1,-1} &= \hbar\Omega(n+1) + \sqrt{2g^2(3+2n)}, \end{aligned}$$

[6]Note that the n indicating the photon number of a state vector does not coincide with the n in the matrix of the time evolution operator (2.60). The latter is the index used to count the subspaces of the *Hilbert* space. Each subspace contains states with three different photon numbers. Therefore $\mathscr{R}_n$ is the same for all states with a given subspace.

corresponding to a total spin singlett and triplet. Note that the second index of the energy eigenvalues E does not correspond to the eigenvalue of the Σ_z-operator, since this is no longer an eigenvalue to an eigenstate of Σ_z.

The time evolution in the rotated basis is given by $U' = \exp(-\frac{i}{\hbar} H'_n\, t)$. We rotate back via $U = T^{-1} U' T$. For the coefficients in the original states this gives

$$\begin{pmatrix} C_{\alpha,\alpha,n}(t) \\ C_{\alpha,\beta,n+1}(t) \\ C_{\beta,\alpha,n+1}(t) \\ C_{\beta,\beta,n+2}(t) \end{pmatrix} = \begin{pmatrix} \frac{n+2+(n+1)\cos(\mathscr{R}_n t)}{3+2n} & i\frac{\sqrt{n+1}\sin(\mathscr{R}_n t)}{\sqrt{2}\sqrt{3+2n}} & \frac{i\sqrt{n+1}\sin(\mathscr{R}_n t)}{\sqrt{2}\sqrt{3+2n}} & \frac{2\sqrt{n+1}\sqrt{n+2}\sin^2(\mathscr{R}_n/2\, t)}{3+2n} \\ \frac{i\sqrt{n+1}\sin(\mathscr{R}_n t)}{\sqrt{2}\sqrt{3+2n}} & \cos^2(\mathscr{R}_n/2\, t) & \sin^2(\mathscr{R}_n/2\, t) & \frac{i\sqrt{n+2}\sin(\mathscr{R}_n t)}{\sqrt{2}\sqrt{3+2n}} \\ \frac{i\sqrt{n+1}\sin(\mathscr{R}_n t)}{\sqrt{2}\sqrt{3+2n}} & \sin^2(\mathscr{R}_n/2\, t) & \cos^2(\mathscr{R}_n/2\, t) & \frac{i\sqrt{n+2}\sin(\mathscr{R}_n t)}{\sqrt{2}\sqrt{3+2n}} \\ \frac{2\sqrt{n+1}\sqrt{n+2}\sin^2(\mathscr{R}_n/2\, t)}{3+2n} & \frac{i\sqrt{n+2}\sin(\mathscr{R}_n t)}{\sqrt{2}\sqrt{3+2n}} & \frac{i\sqrt{n+2}\sin(\mathscr{R}_n t)}{\sqrt{2}\sqrt{3+2n}} & \frac{n+1+(n+2)\cos(\mathscr{R}_n t)}{3+2n} \end{pmatrix} \cdot \begin{pmatrix} C_{\alpha,\alpha,n}(0) \\ C_{\alpha,\beta,n+1}(0) \\ C_{\beta,\alpha,n+1}(0) \\ C_{\beta,\beta,n+2}(0) \end{pmatrix}, \tag{2.60}$$

with $\mathscr{R}_n = g\sqrt{2}\sqrt{3+2n}$.

As in the one-atom case, *Rabi*-oscilations are observed if at least one atom is initially excited or there is at least one photon in the cavity. Differences with respect to the development of the fully excited and ground states. In the single emitter case, the system always fully relaxes to the ground state during one period of the time evolution. This is not the case in the two emitter case, where the maximum occupation probability of the ground state is <1, if the system is initialized fully excited. Analogously, the occupation probability of the fully excited atomic state is always <1, if the system is in the ground state in the beginning.

We will now present the theory used for the description of dissipation. Since the description is formulated in terms of the density matrix formalism this is introduced first.

2.3 The Density matrix

In this chapter the density matrix will be introduced. It is needed where a characterization of the quantum mechanical states of a system in terms of wave functions is either not possible or less convenient. If the density matrix of a system is known, it is possible to compute the expectation value of any given operator. In this sense the density matrix fully characterizes the quantum mechanical state of a system.

Formally, a density operator is defined by three conditions

1. it is self-adjoint,

2. it is positive semi-definite,

3. it has trace 1.

To get a more physical picture, we will discuss two examples. First, we will show how to construct the density matrix for a two-level system in a pure state. Then we show how to treat a state of a two level system, that can not be described by a wave function. The latter case is also referred to as the system state being a mixture.

2.3.1 Pure states and mixtures

Given a basis $\{|\alpha\rangle,|\beta\rangle\}$ of a two level system any state $|\Psi\rangle$ can be expressed as

$$|\Psi\rangle = c_1|\alpha\rangle + c_2|\beta\rangle. \tag{2.61}$$

We next define the projection operator onto the state $|\Psi\rangle$:

$$P = |\Psi\rangle\langle\Psi|. \tag{2.62}$$

This already is the density operator, since it can be used to compute the expectation value of any operator O in the state $|\Psi\rangle$ (see below). We can express it in the basis $\{|\alpha\rangle,|\beta\rangle\}$ as

$$\rho = \sum_{i\in\alpha,\beta}\sum_{j\in\alpha,\beta} |i\rangle\langle i|\Psi\rangle\langle\Psi|j\rangle\langle j| = \begin{pmatrix} c_1c_1^* & c_1c_2^* \\ c_2c_1^* & c_2c_2^* \end{pmatrix} = \begin{pmatrix} \rho_{1,1} & \rho_{1,2} \\ \rho_{2,1} & \rho_{2,2} \end{pmatrix}. \tag{2.63}$$

Note that the diagonal elements are strictly positive and represent the probability of finding the system in state $|\alpha\rangle$ or $|\beta\rangle$, respectively. The off-diagonal terms may be complex and are referred to as transition amplitudes. They are non-zero if the state that is used for constructing the density matrix is a superposition with respect to the basis used for ρ.

Given a basis of the *Hilbert* space of any physical system, the above scheme may be applied to generate ρ. Note that ρ is, in general, not finite dimensional.

So far no information has been gained or lost by describing the system using a density matrix. $|\Psi\rangle$ can be reconstructed from ρ.

If a state of type (2.61) is subject to a measurement yielding either state $|\alpha\rangle$ *or* $|\beta\rangle$, the system state after the measurement can no longer be expressed as a wave-function. This process can be described mathematically by the projection of the state $|\Psi\rangle$ either onto $|\alpha\rangle$ or $|\beta\rangle$, the relative probabilities given by the squared modulus of the coefficients in the superposition:

$$P' = |c_1|^2|\alpha\rangle\langle\alpha| + |c_2|^2|\beta\rangle\langle\beta|. \tag{2.64}$$

This is the density operator of the system after the measurment. In the basis $\{|\alpha\rangle,|\beta\rangle\}$ the matrix form of ρ is given by:

$$\rho = \begin{pmatrix} c_1c_1^* & 0 \\ 0 & c_2c_2^* \end{pmatrix} = \begin{pmatrix} \rho_{1,1} & \rho_{1,2} \\ \rho_{2,1} & \rho_{2,2} \end{pmatrix}. \tag{2.65}$$

Note the difference between (2.63) and (2.65). The measurement induced collapse of the superposition is reflected in the disappearance of the off-diagonal terms.

When an operator O is applied while the state of the system is a mixture, its expectation value will either be $\langle\alpha|O|\alpha\rangle$ or $\langle\beta|O|\beta\rangle$, depending on what state the system actually is in. But since we do not know what state is present, the expectation value $\langle O\rangle$ will be given by the weighted average:

$$\langle O\rangle = |c_1|^2\langle\alpha|O|\alpha\rangle + |c_2|^2\langle\beta|O|\beta\rangle.$$

This can be expressed by means of the density matrix, when O is expressed in the same basis, by forming the trace:

$$\langle O\rangle = tr\{\rho\, O\} \tag{2.66}$$

It can be shown, that the above relation holds for any density matrix and operator. The general form of the density operator, including both examples presented, is:

$$\rho = \sum_n P_n |\Psi_n\rangle\langle\Psi_n|, \tag{2.67}$$

where $|\Psi_n\rangle$ is an arbitrary system state and P_n its statistical weight, satisfying $tr\{\rho\} = 1$.

2.3.2 von-Neumann equation

Just as the *Schrödinger* equation governs the time evolution of state vectors, there is a fundamental differential equation for obtaining the dynamics of the density operator. This equation will be referred to as the *von-Neumann* equation and it can be obtained easily from the *Schrödinger* equation:

$$\begin{aligned} \dot{\rho} &= \sum_n P_n(|\dot{\Psi}\rangle\langle\Psi| + |\Psi\rangle\langle\dot{\Psi}|) && (2.68)\\ &= -\frac{i}{\hbar}\sum_n P_n(H|\Psi\rangle\langle\Psi| + |\Psi\rangle\langle\Psi|H) && (2.69)\\ &= -\frac{i}{\hbar}[H,\rho] && (2.70) \end{aligned}$$

The (numerical) solution of this equation (with some additions discussed in chapter 2.4.2) is one of the main focusses of the present work.

2.3.3 Composite systems and statistical independence

In many cases, a physical system consists of a number of well defined subsystems. In the case of the single-atom *Jaynes-Cummings* Hamiltonian the two-level atomic system and the field mode define two such subsystems.

This structure is reflected in the density matrix. If one is only interested in the dynamics of a given subsystem, the influence of other components can be eliminated. The information about the sub-system is extracted by computing an expectation value of an operator. Given that the operator O^S acts only on a sub-system S, the states $\{|S\rangle\}$ form a basis of the possible system

states and $\{|R\rangle\}$ is a basis of the rest of the system the matrix elements of O_S are given by:

$$O^S_{S,R;S',R'} = O^s_{S,S'}\delta_{R,R'}. \tag{2.71}$$

For the expectancy value $\langle O^S\rangle$ this means:

$$\begin{aligned}\langle O^S\rangle = tr_R\{\rho\, O^S\} &= \sum_{S,S',R,R'} \rho_{S,R;S',R'}\, O^S_{S',R';S,R} \\ &= \sum_{S,S',R,R'} \rho_{S,R;S',R'}\, O^s_{S,S'}\delta_{R,R'} \\ &= \sum_{S,S',R} \rho_{S,R;S',R}\, O^s_{S,S'} \\ &= \sum_{S,S'} tr_R\{\rho\}\, O^s_{S,S'} \\ &= tr\{\rho_S\, O^S\}\end{aligned} \tag{2.72}$$

In the *Jaynes-Cummings* case, if one wants to know the probability of finding the atomic system in the excited state, one must sum up the probability for the atom being excited over all possible states of the field mode.

If two subsystems interact, this is reflected in the dynamics of the respective density matrix. There is a criterion for the independence of subsystems. It is shown in statistics that, if two events A and B are independent, the probability of $A \cap B$ is given by $p_A \cdot p_B$, where p_i is the probability of the respective event. An analogous assertion holds for the case of density operators. If a set of physical systems $A, B, C...$ does not interact, its composite density matrix will factorize at any time:

$$\rho(t) = \rho_A(t) \otimes \rho_B(t) \cdots$$

If one observes that the composite density matrix of a system can not be reconstructed from the subsystem density matrices, this shows that the two sub-systems exhibit interactions.

2.3.4 The Jaynes Cummings system in the density matrix formalism

At the end of the chapter, the *von Neumann* equation for the one atom *Jaynes-Cummings* system is presented.

We first insert (2.37) into (2.70). In order to arrive at equations for the elements of ρ, we must evaluate the commutator. Due to the block-diagonal structure of H, only elements form 2×2 –sub matrices are connected. For a given index n the commutator is:

$$\dot{\rho}_{\alpha\, n;\alpha\, n} = -i\sqrt{n+1}(g\rho_{\beta\, n+1;\alpha\, n} - g^*\rho_{\alpha\, n;\beta\, n+1}) \tag{2.73}$$

$$\dot{\rho}_{\alpha\, n;\beta\, n+1} = -i(\delta\, \rho_{\alpha\, n;\beta\, n+1} + g^*\sqrt{n+1}(\rho_{\beta\, n+1;\beta\, n+1} - \rho_{\alpha\, n;\alpha\, n}))\tag{2.74}$$

$$\dot{\rho}_{\beta\, n+1;\alpha\, n} = \quad i(\delta\, \rho_{\beta\, n+1;\alpha\, n} + g\sqrt{n+1}(\rho_{\beta\, n+1;\beta\, n+1} - \rho_{\alpha\, n;\alpha\, n}))\tag{2.75}$$

$$\dot{\rho}_{\beta\, n+1;\beta\, n+1} = \quad i\sqrt{n+1}(g\rho_{\beta\, n+1;\alpha\, n} - g^*\rho_{\alpha\, n;\beta\, n+1}) \tag{2.76}$$

The solution of these equations can be obtained from (2.49) keeping in mind the structure of the density matrix as given in (2.63). The diagonal terms are driven by the off-diagonal terms and vice versa. This leads to the observed oscillatory behavior. It also becomes clear that a disappearance of the off-diagonal terms leads to static values of the diagonal terms.

This happens as a consequence of dissipation, a phenomenon that we want to turn our attention to next.

2.4 Dissipation

The *Jaynes-Cummings* system presented in the previous chapters exhibits a typically quantum mechanical behavior: if the state of the system is a coherent superposition, it remains so for all times. In experiments such dynamics are usually not observed. Coherence is lost by the interaction of the system and its surroundings. This effect is modeled by coupling the *Jaynes-Cummings* system to a so called bath; a concept known from thermodynamics. A bath is supposed to be a system with a great number of degrees of freedom and a broad, continuous spectrum. It must only weakly interact with the system it is coupled to, so that a system description neglecting the interaction remains accurate. It will be seen that such a system-bath interaction causes loss of coherence for the *Jaynes-Cummings* states, i.e. , *Rabi* flopping is not observed for all times anymore.

Dissipation can be incorporated into a system description in different ways. Here we present a way of finding additional terms for the *von-Neumann* equation of the system. These are known as *Lindblad* terms and they have the

advantage over phenomenological decay processes of being trace conserving while still being are conceptually efficient. After deriving them, we will specify what terms will be added to the model.

2.4.1 Lindblad terms

Consider the Hamiltonian

$$H = H_0 + H_I = H_S + H_R + H_I, \tag{2.77}$$

where H_0 describes the sum of system and bath Hamiltonian, H_S and H_B, and H_I the interaction between system and bath. The *von-Neumann* equation in the interaction picture is

$$\frac{\partial \tilde{\rho}}{\partial t} = -\frac{i}{\hbar}[\tilde{H}_I(t), \tilde{\rho}(t)]. \tag{2.78}$$

By the procedure described in Appendix (A), this can be approximated by:

$$\frac{\partial \tilde{\rho_S}}{\partial t}(t) = \sum_\alpha \frac{\kappa_\alpha}{2}(2\tilde{s}_\alpha(t)\tilde{\rho_S}(t)\tilde{s}_\alpha^\dagger(t) - \tilde{\rho_S}(t)\tilde{s}_\alpha^\dagger(t)\tilde{s}_\alpha(t) - \tilde{s}_\alpha^\dagger(t)\tilde{s}_\alpha(t)\tilde{\rho_S}(t)) \tag{2.79}$$

which reads

$$\frac{\partial \rho_S}{\partial t} = -\frac{i}{\hbar}[H_S, \rho_S] + \sum_\alpha \frac{\kappa_\alpha}{2}(2s_\alpha\rho_S s_\alpha^\dagger - \rho_S s_\alpha^\dagger s_\alpha - s_\alpha^\dagger s_\alpha \rho_S) \tag{2.80}$$

in the *Schrödinger* picture.

The second term on the RHS of (2.80) for one α is referred to as *Lindblad* term. *Lindblad* terms are trace-conserving as can be seen from the cyclic invariance of the trace operation:

$$\frac{\partial\, tr\{\rho_S\}}{\partial t}|_{LB} = \sum_\alpha \frac{\kappa_\alpha}{2}(2tr\{s_\alpha\rho_S s_\alpha^\dagger\} - tr\{\rho_S s_\alpha^\dagger s_\alpha\} - tr\{s_\alpha^\dagger s_\alpha \rho_S\}) \tag{2.81}$$

$$= \sum_\alpha \frac{\kappa_\alpha}{2}(2\, tr\{s_\alpha\rho_S s_\alpha^\dagger\} - 2\, tr\{s_\alpha\rho_S s_\alpha^\dagger\}) = 0 \tag{2.82}$$

In addition, *Lindbald* terms conserve hermiticity. This can be shown by forming the hermitian conjugate and keeping in mind that one must reverse the order of the operators in a product, conjugating each for itself and that ρ itself is hermitian.

2.4.2 Dissipative terms in the model

Now that we have a way to account for dissipation in our model, we select a set of dissipative terms to include, and explain why they are physically significant. In addition, we give analytical results where possible in order to be able to asses the quality of the numerics.

Cavity losses

In the *Jaynes-Cummings* model the field mode studied is restricted to a finite volume that can be viewed as a resonator. A certain number of photons always leaves this volume at a given rate in a true physical system. This effect is accounted for in the model by the following term

$$\frac{\partial \rho}{\partial t}|_{Cav} = \frac{\kappa}{2}(2b\rho b^\dagger - \rho b^\dagger b - b^\dagger b\rho), \tag{2.83}$$

where we have introduced the cavity constant κ. The cavity losses are present in order for the system to relax to the ground state.

It is possible to evaluate the contributions to for the density matrix elements for certain initial conditions. Since the atomic part of ρ is left unchanged, we will compute the solution only for the density matrix of the photonic system. For the matrix elements of ρ we get:

$$\begin{aligned} \dot{\rho}_n|_{cav} &= \frac{\kappa}{2}\langle n,m|2b\rho b^\dagger - \rho b^\dagger b - b^\dagger b\rho|m\rangle \\ &= \kappa\sqrt{(n+1)(m+1)}\,\rho_{n+1,m+1} - \frac{\kappa}{2}(m+n)\,\rho_{n,m}. \end{aligned} \tag{2.84}$$

Note that only elements lying on the same line parallel to the diagonal are coupled. It can be shown that the dynamics induced upon ρ by (2.84) lead to a decay of all matrix elements but the ground state occupation probability which must go to 1 due to trace conservation[7]. This is the characteristic dephasing effect found in all system-reservoir interactions. As a consequence states that are originally superpositions with respect to the eigenbasis of the density matrix, are turned into a mixture of different states with no superpositions present anymore.

[7] This can be seen by applying *Gershgorin's* theorem, cf (6).

For the diagonal elements the differential equation reduces to

$$\frac{1}{\kappa}\dot{\rho}_n = (n+1)\,\rho_{n+1} - n\,\rho_n, \tag{2.85}$$

where we have dropped the second index. The solution to (2.88) is given by:

$$p(x,t) = p_0\,(1 - e^{-\kappa t} + x\,e^{-\kappa t}). \tag{2.86}$$

This can be seen by rewriting (2.85) as a partial differential equation for the function

$$p(x,t) = \sum_n \rho_n\,x^n, \tag{2.87}$$

leading to

$$\frac{1}{\kappa}\frac{\partial p}{\partial t} = (1-x)\frac{\partial p}{\partial x}. \tag{2.88}$$

The condition $tr\{\rho(t)\} = 1$ implies that $p(1,t) = p_0 = \sum_n \rho_n = 1$. In order to recover the density matrix elements, one must rewrite(2.86) as a power series. Choosing $p_0 = \exp(\alpha(x-1))$, satisfying the above condition, makes this possible. This choice corresponds to the initial state of the photonic system being *Poisson* distributed, i.e., a coherent state: $\rho_n = \frac{\alpha^n}{n!}e^{-\alpha}$. We finally have:

$$p(x,t) = \exp\left(\alpha\,e^{-\kappa t}\,(x-1)\right) = \exp\left(-\alpha\,e^{-\kappa t}\right)\cdot\sum_{j=0}^{\infty}\frac{(\alpha\,e^{-\kappa t})^n}{n!}x^n.$$

For the the elements of ρ this means:

$$\rho_{n,n}(t) = \frac{(\alpha\,e^{-\kappa t})^n}{n!}\cdot e^{\left(-\alpha\,e^{-\kappa t}\right)}. \tag{2.89}$$

The decay is fastest for high photon-numbers.

Spontaneous emission into non-lasing modes

Emission of radiation from the atomic system can take place not only into the mode entering the *Jaynes-Cummings* Hamiltonian. To account for these

emission processes within the system model, excited atom-states are deexcited with a certain probability. These processes are referred to emission into non-lasing modes. The corresponding *Lindblad* term is:

$$\frac{\partial \rho}{\partial t}|_{nl} = \frac{1}{2\,\tau_{nl}}(2\sigma_-\rho\sigma_+ - \rho\sigma_+\sigma_- - \sigma_+\sigma_-\rho). \tag{2.90}$$

The photonic degrees of freedom are not involved in this process and therefore only the density matrix of the atomic system ($n_{atoms} = 1$) will be considered in the following analytical treatment. In matrix form the differential equations for the matrix elements of ρ read:

$$\begin{pmatrix} \dot{\rho}_{\alpha,\alpha} \\ \dot{\rho}_{\alpha,\beta} \\ \dot{\rho}_{\beta,\alpha} \\ \dot{\rho}_{\beta,\beta} \end{pmatrix} = \frac{1}{2\,\tau_{nl}} \begin{pmatrix} -1 & 0 & 0 & 0 \\ 0 & -1/2 & 0 & 0 \\ 0 & 0 & -1/2 & 0 \\ 1 & 0 & 0 & 0 \end{pmatrix} \begin{pmatrix} \rho_{\alpha,\alpha} \\ \rho_{\alpha,\beta} \\ \rho_{\beta,\alpha} \\ \rho_{\beta,\beta} \end{pmatrix}. \tag{2.91}$$

Given that all matrix elements are initially set to 1 the solutions to this set if equations is given by[8]

$$\begin{aligned} \rho_{\alpha,\alpha}(t) &= e^{-\frac{1}{\tau_{nl}}t}, \\ \rho_{\alpha,\beta}(t) &= e^{-\frac{1}{2\tau_{nl}}t}, \\ \rho_{\beta,\alpha}(t) &= e^{-\frac{1}{2\tau_{nl}}t}, \\ \rho_{\beta,\beta}(t) &= (1 - e^{-\frac{1}{\tau_{nl}}t}). \end{aligned}$$

Again, an exponential decay of the off-diagonal terms is observed that leads to decoherence of the system. In addition the excited state exhibits an exponential decay that leads to a buildup of the ground state. For $t \to \infty$ only $\rho_{\beta,\beta}$ remains non-zero.

Pumping

In many experiments energy is delivered to the atomic system via a so called pumping process. Radiation enters the resonator leading to a transition of

[8] This initial condition is most convenient yet the resulting matrix does not represent a density matrix since it has a trace of 2.

the atoms into the excited state. It is possible to pump with light that does not have the frequency of the cavity mode, by pumping into states not included in the two-level description. The *Lindblad* terms read:

$$\frac{\partial \rho}{\partial t}|_{nl} = \frac{P}{2}(2\sigma_+\rho\sigma_- - \rho\sigma_-\sigma_+ - \sigma_-\sigma_+\rho). \tag{2.92}$$

The parameter P is the pump-rate. The process is reciprocal the the emission into non-lasing modes. As a consequence the analytical results are the same as for emission , only the excited and deexcited states must be swapped:

$$\begin{aligned}
\rho_{\beta,\beta}(t) &= e^{-Pt}, \\
\rho_{\alpha,\beta}(t) &= e^{-\frac{P}{2}t}, \\
\rho_{\beta,\alpha}(t) &= e^{-\frac{P}{2}t}, \\
\rho_{\alpha,\alpha}(t) &= (1 - e^{-Pt}).
\end{aligned}$$

A comparison between the analytical results presented here and the numerical data is given in 3.1.

2.5 Many-atom Jaynes Cummings model with Born-Markov dissipation

Now that all parts of the models have been described, we formulate the differential equation that is the focus of the current work. The *von Neumann* equations of motion for the density operator ρ of a many-atom *Jaynes–Cummings* system, including all the dissipative terms introduced in section 2.4.2 is

$$\begin{aligned}
\frac{\partial}{\partial t}\rho(t) = & -\tfrac{i}{\hbar}[H_J C, \rho(t)] \\
& + \frac{\kappa}{2}(2b\rho b^\dagger - \rho b^\dagger b - b^\dagger b\rho\,) \\
& + \frac{1}{2\,\tau_{nl}}(2\sigma_-\rho\sigma_+ - \rho\sigma_+\sigma_- - \sigma_+\sigma_-\rho) \\
& + \frac{P}{2}(2\sigma_+\rho\sigma_- - \rho\sigma_-\sigma_+ - \sigma_-\sigma_+\rho),
\end{aligned} \tag{2.93}$$

where the Hamiltonian H_{JC} is the many-atom Hamiltonian including inhomogeneous broadening (2.55). The properties of this model are explored for several different parameter sets. The main focus lies on the study of superradiant enhancement of spontaneous emission. The theory of the effect is presented in the following section. The results are reported in chapter 3.2.

2.6 Superradiance

The concept of superradiance was introduced by R. H. Dicke in 1954 (5). In his original work, the emission of radiation by a small volume of gas molecules is considered. Under certain conditions, the radiation originating from a group of initially excited molecules does not scale linearly with the molecule number. In some cases collective effects lead to an enhancement of the radiation process, such that its maximum intensity scales quadratically with the number of molecules. *"For want of a better term, a gas which is radiating strongly because of coherence"* is referred to as being *"superradiant"* by Dicke. But the opposite effect can also be observed: the presence of many atoms may decrease or inhibit the emission of radiation as compared to an N-fold multiple of single molecules. Such states may be termed subradiant or dark states. Both, superradiant and subradiant effects have been observed experimentally.

Dicke studied phenomena relating to nuclear magnetic resonance of molecules and atoms with transition frequencies in the MHz region. Therefore the assumption of all particles experiencing the same field was justified for systems having a comparably large spatial extent. Today, superradiance has again started to draw attention at a different length-scale. With the availability of densely packed quantum-dots and transition energies in the region of THz, the same phenomenon may now play a role at energies several orders of magnitude greater. But it is difficult to separate the numerous effects taking place in the light matter interaction of quantum-dots. Therefore the understanding and, if possible, isolation of superradiance induced phenomena in quantum dots is essential to quantify its contribution to the overall picture.

In a first step, collective atomic states and their description in terms of *Dicke* states (see below) will be introduced. Then the emergence of superradi-

ance will be demonstrated in this basis as well as in a basis of product-states. After comparing similarities and differences of these two cases, we will turn to possibilities of quantifying the amount of superradiance a given system is exhibiting at a certain time.

2.6.1 Dicke states

Recall the N-atom *Jaynes-Cummings* Hamiltonian discussed in chapter 2.2:

$$H = \hbar\omega\Sigma_z + \hbar\Omega b^\dagger b + \hbar(gb\Sigma_+ + g^* b^\dagger \Sigma_-). \tag{2.94}$$

This equation looks very much like its single-atom pendant, but the fact that the single-atom "spin" operators have been replaced by their many-atom counterparts leads to the emergence of superradiant behavior. Note that the interaction of all atoms with the same field mode is essential for the Hamiltonian to be so readily generalized.

In the description of real QD systems one most take into account the effect of statistical variation of the transition frequencies of the dots. This can be incorporated by relaxing the condition that ω is identical for all atoms. This leads to the Hamiltonian

$$H = \hbar \sum_{i=1} N\omega_i \sigma_{z,i} + \hbar\Omega b^\dagger b + \hbar(gb\Sigma_+ + g^* b^\dagger \Sigma_-). \tag{2.95}$$

The theoretical treatment of (2.95) is beyond the scope of this work. References can be found in (14). Numerical results for different magnitudes of inhomogeneous broadening are presented in chapter 3.2. We now turn again to the discussion of the non-broadened case.

The Σ-operators have the same commutation relations as the operators of total angular momentum[9]. Therefore, the well known techniques of angular momentum algebra can be applied to this case of light matter interaction. The central aspect is that the many-atom Hamiltonian (2.94) commutes with the operator Σ^2. This operator is defined as

$$\Sigma^2 = \Sigma_x^2 + \Sigma_y^2 + \Sigma_z^2. \tag{2.96}$$

[9]The commutation relations are given in C

This may be rewritten as

$$\Sigma^2 = \Sigma_z^2 + \tfrac{1}{2}(\Sigma_+\Sigma_- + \Sigma_-\Sigma_+). \tag{2.97}$$

The fact that it commutes with the system Hamiltonian makes the eigenvalues of this operator a new good quantum number; the analogon to the quantum number of total angular momentum. It is this new quantum number that provides the basis for the description of super- and subradiant effects. In order to make this clear, we first introduce a suitable basis: the simultaneous eigenstates of Σ_z and Σ^2.

With m denoting the eigenvalues of Σ_z and $l(l+1)$ those of Σ^2, we can express this in the usual notation as:

$$\Sigma_z|l,m\rangle = m|l,m\rangle \tag{2.98}$$
$$\Sigma^2|l,m\rangle = l(l+1)|l,m\rangle. \tag{2.99}$$

These states are referred to as *Dicke* states. The set of eigenvalues is known to obey the conditions:

$$l = 0, \tfrac{1}{2}, 1, \tfrac{3}{2}, \ldots$$
$$|m| \leq l.$$

The energy of the atomic sub-system is connected to m by

$$E_A = \hbar\omega m.$$

This can be, at most, equal to $E_{max} = \hbar\frac{N}{2}\omega$ with all atoms in the excited state. Since m can be, at most, equal to l, we have an upper bound for l:

$$l \leq \tfrac{N}{2}.$$

The effect of the raising- and lowering operators is known to be:

$$\Sigma_+|l,m\rangle = \sqrt{(l-m)(l+m+1)}|\, l,m+1\rangle, \tag{2.100}$$
$$\Sigma_-|l,m\rangle = \sqrt{(l+m)(l-m+1)}|\, l,m-1\rangle. \tag{2.101}$$

Here the property of l being a good quantum number – in contrast to m – under the dynamics of the many-atom Hamiltonian (2.94) can be observed. No matter what combination of raising- and lowering-operators is applied,

l remains constant. This is connected to the properties of the light-matter interaction, as can be seen intuitively by taking a second look at the definition of Σ^2 in (2.97). Reading the equation in terms of expectation values, one can see that the sum

$$\langle \Sigma_z^2 \rangle + \tfrac{1}{2}(\langle \Sigma_+ \Sigma_- \rangle + \langle \Sigma_- \Sigma_+ \rangle) \tag{2.102}$$

is constant. If the system is initialized at full inversion and then radiating energy, the expectancy value of Σ_z^2 is reduced until the energy of the atomic sub system is zero. This leads to an increase of the mean value of the other term, involving products of the operators modeling the light-matter interaction. Although it is not possible to quantify this effect it is clear that a change in the interaction is likely to be observed.

2.6.2 Superradiance in Dicke states

To understand how the light-matter interaction is altered by many-atom effects, we consider the probability of emission of a photon in a *Dicke* state $|l, m\rangle$, given that the field is initially in the vacuum state $|0\rangle$. The transition rates according to *Fermi's* golden rule are:

$$R_{trans} = \frac{2\pi}{\hbar} |\langle \Psi_f | H_I | \Psi_i \rangle|^2 D(\omega), \tag{2.103}$$

where $\Psi_{f/i}$ refer to the final and initial state of the system and $D(\omega)$ is the density of states (DOS) for the photons in the resonator. H_I is the interaction Hamiltonian, in our case the dipole operator in RWA. Note that the Ψ_i must be eigenstates of the unperturbed system for the rule to be applicable. Due to energy conservation the only possible final state is $|l, m-1\rangle|1\rangle$. An additional complication is introduced by the fact that emission does not take place into a continuum of modes, the latter being a prerequisite for applying *Fermi's* golden rule. To correct this, we take into account the effect of cavity losses, leading to a finite lifetime of the field state $|1\rangle$ and thereby providing a continuous mode spectrum. As can be seen from the differential equation for the matrix elements due to cavity losses in (2.84), the state will decay at a rate κ. Therefore our DOS is be given by:

$$D(\omega) = \frac{1}{\pi\hbar} \frac{\kappa}{(\omega - \omega_{res})^2 + \kappa^2}, \tag{2.104}$$

introducing a factor of κ^{-1} in the transition rate at resonance. This leads to:

$$R_{trans} = \frac{2|g|^2}{\kappa}|\langle l, m-1|\langle 1|\Sigma_- b^\dagger|0\rangle|l, m\rangle|^2 \tag{2.105}$$

$$= \frac{2|g|^2}{\kappa}[l^2 + l - m^2 + m] \tag{2.106}$$

We can transfer this to units of radiation by introducing the proportionality constant I_0 that corresponds to the intensity of radiation by a single emitter. We then have

$$I = I_0[l^2 + l - m^2 + m]. \tag{2.107}$$

This is the result obtained by Dicke (5). From equation (2.107) we see the radiation is greatest for $l = N/2$ and $m = 0$:

$$I_{max} = I_0 \tfrac{1}{2}N(\tfrac{1}{2}N + 1). \tag{2.108}$$

Note that this corresponds to the system being *half* excited. In the fully excited case $m = \frac{N}{2}$ the rate is:

$$I_{inv} = I_0 N, \tag{2.109}$$

corresponding only to a linear scaling with the number of atoms. A striking behavior is observed for $l = m = 0$, for which the transition rate vanishes. No radiation is expected to be observed, although the atomic system is half excited.

The dependence of the observed radiance on the quantum number l led Dicke to refer to it as the *cooperation number*. For $l = 0$ no radiation is observed, even if the system is in a half excited state. Such a *Dicke* state is referred to as dark. In general, cooperative effects that lead to a decrease in the emission are referred to as *subradiant*. Especially the emergence of dark states is quite counter-intuitive. One way of looking at this situation in a semi-classical picture is that the radiating atomic dipoles are oppositely phased and the radiation of one atom is immediately absorbed by the other. But note that the expectation value of the dipole operator is zero in any given *Dicke* state

$$\langle l, m|\hbar g^* \Sigma_- + \hbar g \Sigma_+|l, m\rangle = \hbar(g^*\langle l, m|l, m-1\rangle + g\langle l, m|l, m+1\rangle) \tag{2.110}$$

$$= 0, \tag{2.111}$$

since *Dicke* states are orthogonal. This is not the case for the squared dipole operator, corresponding to the variance, since the mean value vanishes:

$$\langle l,m|\left(\hbar g^{*}\Sigma_{-}+\hbar g\Sigma_{+}\right)^{2}|l,m\rangle = \hbar^{2}|g|^{2}\langle l,m|\Sigma_{+}\Sigma_{-}+\Sigma_{-}\Sigma_{+}|l,m\rangle \tag{2.112}$$

$$= 2\hbar^{2}|g|^{2}\langle l,m|\Sigma^{2}-\Sigma_{z}^{2}|l,m\rangle \tag{2.113}$$

$$= 2\hbar^{2}|g|^{2}\left[l(l+1)-m^{2}\right], \tag{2.114}$$

where we have used the definition of Σ^2 in (2.97). Again, the expectancy value is greatest for $m = 0$ and $l = \frac{N}{2}$. It seems worthy to note that this is analogous to the photon field giving rise to spontaneous emission. In a given field state $|n\rangle$ the field expectancy value vanishes, while the variance does not.

2.6.3 Superradiance in atomic product states

Although *Dicke* states are very useful in a theoretical treatment of superradiance, they can not be easily realized in experiments. Therefore we will give a perturbative account of the emission probability of a system of N atoms, provided the system is initially in a state:

$$|\Phi\rangle = \Pi_{j=1}^{N}\left(c_{1}|\alpha\rangle + c_{2}|\beta\rangle\right), \tag{2.115}$$

where $|\alpha,\beta\rangle$ represent the excited and ground states of the single atom. It is assumed that all atoms are in the same coherent superposition of the excited and the ground-state. The coefficients are complex numbers satisfying the normalization condition $|c_1|^2+|c_2|^2 = 1$. The application of *Fermi's* golden rule is not possible here since the superpositions generating the product states are not eigenstates of the non-interacting light-matter system. Therefore a different scheme is applied by Mandel and Wolf in (10) that we will adopt.

Given that the photon field is initially in the ground state $|0\rangle$, the initial density matrix is:

$$\rho(0) = |\Phi\rangle\langle\Phi| \otimes |0\rangle\langle 0|$$

We are now interested in the probability P_e to find the system in a state where a photon has been emitted by the atomic system after a time δt. This probability for this is given by the sum over all diagonal elements with the

field in state $|1\rangle$ of the density matrix $\rho(\delta t)$. This means that one must sum over all states Ψ_A of the atomic system:

$$P_e(\delta t) = \sum_{\text{all}A} \langle \Psi_A | \langle 1 | \rho(\delta t) | 1 \rangle \Psi_A \rangle \tag{2.116}$$

We use a *Born*–type approximation[10] for the density matrix at time δt. The probability of the system being in a state Ψ is then given by:

$$P_e(\Psi, \delta t) = \tfrac{1}{\hbar^2} \int_0^{\delta t} \int_0^{t_1} \langle \Psi | H_I(t_1) \rho(0) H_I(t_2) | \Psi \rangle + h.c.\, dt_2 dt_1, \tag{2.117}$$

where $H_I(t)$ refers to the interaction Hamiltonian in the interaction picture. It is given by:

$$H_I(t) = g^* \Sigma_- e^{-i\omega t} b^\dagger e^{i\Omega t} + g \Sigma_+ e^{-i\omega t} b e^{-i\Omega t} \tag{2.118}$$

$$:= g^* \Sigma_-(t) b^\dagger(t) + g \Sigma_+(t) b(t) \tag{2.119}$$

Substituting the approximation (2.117) for ρ and the interaction Hamiltonian (2.118) into the expression for the transition probability (2.116), we arrive at:

$$\begin{aligned}
P_e(\delta t) =& \tfrac{1}{\hbar^2} \int_0^{\delta t} \int_0^{t_1} \sum_{allA} \langle \Psi_A | \langle 1 | \left(\hbar (g b(t_1) \Sigma_+(t_1) + g^* b_I^\dagger(t_1) \Sigma_-(t_1) \right) |\Phi\rangle\langle\Phi| \otimes \cdots \\
& |0\rangle\langle 0| \hbar \left(g b(t_2) \Sigma_+(t_2) + g^* b_I^\dagger(t_2) \Sigma_-(t_2) \right) |1\rangle |\Psi_A\rangle + h.c.\, dt_2 dt_1 \\
=& |g|^2 \int_0^{\delta t} \int_0^{t_1} \sum_{allA} \langle \Phi | \Sigma_+(t_2) | \Psi_A \rangle \langle \Psi_A | \Sigma_-(t_1) | \Phi \rangle \\
& \langle 1 | b^\dagger(t_1) | 0 \rangle \langle 0 | b(t_2) | 1 \rangle + h.c.\, dt_2 dt_1 \\
=& |g|^2 \int_0^{\delta t} \int_0^{t_1} \langle \Phi | \Sigma_+ \Sigma_- | \Phi \rangle\, e^{-i\omega(t_1 - t_2)}\, e^{i\Omega(t_1 - t_2)} + h.c.\, dt_2 dt_1 \\
=& 2|g|^2 \langle \Phi | \Sigma_+ \Sigma_- | \Phi \rangle \int_0^{\delta t} \int_0^{t_1} \frac{e^{i(\Omega-\omega)(t_1-t_2)} + e^{-i(\Omega-\omega)(t_1-t_2)}}{2} dt_2 dt_1 \\
=& 2|g|^2 \langle \Phi | \Sigma_+ \Sigma_- | \Phi \rangle \left(\frac{1 - \cos[(\Omega - \omega)\delta t]}{(\Omega - \omega)^2} \right) \\
=& |g|^2 \langle \Phi | \Sigma_+ \Sigma_- | \Phi \rangle \left(\frac{\sin[(\frac{\Omega-\omega}{2})\delta t]}{\frac{1}{2}(\Omega - \omega)} \right)^2 .
\end{aligned} \tag{2.120}$$

[10] See chapters 16.6.2 and 14.1.1 in (10)

Since we are interested in a transition *rate* we differentiate with respect to time leading to:

$$\frac{\partial}{\partial \delta t} P_e = |g|^2 \langle \Phi | \Sigma_+ \Sigma_- | \Phi \rangle \cdot \frac{2 \sin(\frac{\Omega-\omega}{2}\delta t) \cdot \cos(\frac{\Omega-\omega}{2}\delta t)}{\frac{1}{2}(\Omega-\omega)} \tag{2.121}$$

$$= 2|g|^2 \langle \Phi | \Sigma_+ \Sigma_- | \Phi \rangle \cdot \frac{\sin(\Omega-\omega)\delta t}{(\Omega-\omega)}. \tag{2.122}$$

For times δt that are long enough on an atomic time scale, we substitute the sinc-type expression by a δ–distribution. In addition we integrate over all modes according to the DOS (2.104) and arrive at an expression for the transition rates:

$$R_{trans} = \frac{2|g|^2}{\kappa} \langle \Phi | \Sigma_+ \Sigma_- | \Phi \rangle \tag{2.123}$$

$$= \frac{2|g|^2}{\kappa} \left[N|c_2|^2 + N(N-1)|c_2|^2|c_1|^2 \right]. \tag{2.124}$$

With this, we have similar result to the one obtained for the *Dicke* states in section 2.6.2.

For $|c_2|^2 = 1$ and $|c_1|^2 = 0$ we obtain

$$R_{trans} = \frac{2|g|^2}{\kappa} N,$$

the sam as for the fully inverted *Dicke* state $|\frac{N}{2}, \frac{N}{2}\rangle$ in (2.109). Differences occur for the state $|\frac{N}{2}, 0\rangle$ in (2.108) and the product state $|c_2|^2 = \frac{1}{2}$ and $|c_1|^2 = \frac{1}{2}$. The latter is smaller by an amount of $\frac{N}{2}$. Note that there is no combination of c_1 and c_2 that leads to a fully dark product state, aside from the trivial case $|c_1|^2 = 1$. Although having the same emission probabilities, the *Dicke* and product states have distinct properties. We have already seen in (2.110) that the expectancy value of the dipole operator is 0 in any *Dicke* state. This is not the case for all product states:

$$\langle \Phi | g^* \Sigma_- + g \Sigma_+ | \Phi \rangle = g^* c_1^* c_2 + g c_1 c_2^* N \tag{2.125}$$

$$= 2\Re[g\, c_1\, c_2] N. \tag{2.126}$$

Only fully inverted or fully relaxed populations have a vanishing dipole moment. In these cases *Dicke* and product states coincide.

2.6.4 Emission into free space

The *Janyes-Cummings* model incorporates light-matter interaction only for a single field mode. While this is advantageous from a conceptional point of view, it yields problems when computing transition rates. In the above discussion this led to the necessity of introducing cavity losses. A common reference frame for spontaneous emission is a mode density coressponding to free space. The emission rate R is given by ((10), see chapter 15.4):

$$R = A[N|c_2|^2 + N(N-1)|c_2|^2|c_1|^2],$$

where the *Einstein* coefficient A has been introduced.

2.6.5 Time evolution of superradiance

Due to energy conservation, the radiant flux Φ of the atomic system must equal its rate of energy loss at all times[11]. The radiant flux in a product state given by

$$\Phi = \hbar\omega A[N|c_2|^2 + N(N-1)|c_2|^2|c_1|^2], \tag{2.127}$$

while the energy loss is:

$$-\frac{\partial}{\partial t}\langle H_A(t)\rangle = -\hbar\omega\frac{\partial}{\partial t}[N|c_2(t)|^2 - \tfrac{N}{2}] \tag{2.128}$$

$$= -\hbar\omega\, N\,\frac{\partial}{\partial t}|c_2(t)|^2. \tag{2.129}$$

Equating both and using $|c_1|^2 = 1 - |c_2|^2$ leads to the differential equation:

$$\frac{\partial}{\partial t}|c_2(t)|^2 = -AN|c_2|^2[1 - (1 - \tfrac{1}{N})|c_2|^2] \tag{2.130}$$

$$\tag{2.131}$$

which is solved by

$$|c_2(t)|^2 = \frac{N}{N - 1 + e^{AN\,t}}. \tag{2.132}$$

[11] The discussion follows sec. 16.6.3 in (10).

What can be seen at first glance is that in the limit $t \to \infty$ the system will fully relax. The solution – the rate of photon emission from the atomic system – is given by:

$$R(t) = \frac{AN^3 e^{ANt}}{(N-1+e^{ANt})^2}. \tag{2.133}$$

Accordingly, the expectancy value of the Hamiltonian develops as:

$$\langle H_A(t) \rangle = \hbar\omega \frac{N^2}{N-1+e^{ANt}}. \tag{2.134}$$

Note that it has been assumed that the system remains in a product state at all times. This will *not* be the case if the dynamics is ruled by a *Jaynes-Cummings* Hamiltonian. Therefore this time development can only be seen as an approximation. In addition, any process that leads to a decoherence, such as interaction with a thermal bath, will cause the atomic system to evolve away from a product state.

2.6.6 Measures of superradiance

Both treatments of superradiance presented this far – in *Dicke* states in section 2.6.2 and in product states in section 2.6.3 – showed a proportionality between the the emission rate and the expectation value $\langle \Sigma_+ \Sigma_- \rangle$ in the state under consideration. Keeping in mind that both treatments are of second order in the interaction (Born approximation), it is natural that such products will describe the effect on this level, since the interaction is linear in these two operators. We will now take a closer look at the structure of the expectation value $\langle \Sigma_+ \Sigma_- \rangle$ in order to arrive at means to quantify the amout of superradiance a system is exhibiting at a given time.

The operator $\Sigma_+ \Sigma_-$, also known as the squared atomic polarization (14), can be expressed in single-atom operators as

$$\Sigma_+ \Sigma_- = \sum_{i=1}^{N} \sigma_{+,i} \sigma_{-,i} + \sum_{i \neq j} \sigma_{+,i} \sigma_{-,j} \tag{2.135}$$

$$:= \Sigma_+ \Sigma_-^{\text{uncorr}} + \Sigma_+ \Sigma_-^{\text{corr}}. \tag{2.136}$$

It can be seen that there are two distinct contributions, one referred to as the uncorrelated, the other as the correlated component of the operator.

The role of the uncorrelated component can be best seen in a product basis of the type $|\varphi_1, \varphi_2, \cdots\rangle$, $\varphi_i \in \{\alpha, \beta\}$, i.e., a given atom either being fully excited or in the ground state. Applying the uncorrelated part of the operator $\Sigma_+\Sigma_-$ yields

$$\langle \varphi_1, \varphi_2, \cdots | \Sigma_+ \Sigma_-^{\text{uncorr}} | \varphi_1, \varphi_2, \cdots \rangle = N1, \tag{2.137}$$

where $N1$ is the number of excited atoms in the state $|\varphi_1, \varphi_2, \cdots\rangle$. The total number of atoms is $N = N1+N2$, where $N2$ the number of atoms in the ground state. The uncorrelated part is strictly linear in the number of emitters, thus it can not be responsible for any supperradiant contributions, since we expect these to scale in a non-linear fashion as a function of emitter-number. It is related to the energy of the atomic system, which is

$$\langle \varphi_1, \varphi_2, \cdots | \Sigma_z | \varphi_1, \varphi_2, \cdots \rangle = \tfrac{1}{2}(N1 - N2) = N1 - \tfrac{1}{2}N. \tag{2.138}$$

Independent of a specific basis we can conclude that

$$\langle \Sigma_+ \Sigma_- \rangle^{\text{uncorr}} = \langle \Sigma_z \rangle + \tfrac{1}{2}N. \tag{2.139}$$

This will be of some help in finding a physical interpretation of the correlative part. Recall the formula for the expectation value of the squared dipole moment (2.112). Making use of the relation (2.139) we find that the correlated contribution is directly related to the squared dipole moment:

$$\begin{aligned} \langle l, m | \left(\hbar g^* \Sigma_- + \hbar g \Sigma_+\right)^2 | l, m \rangle &= \hbar^2 |g|^2 \langle l, m | \Sigma_+ \Sigma_- + \Sigma_- \Sigma_+ | l, m \rangle && (2.140) \\ &= 2\hbar^2 |g|^2 (\langle l, m | \Sigma_+ \Sigma_-^{\text{corr}} | l, m \rangle \\ &\qquad + \langle l, m | \Sigma_+ \Sigma_-^{\text{uncorr}} - \Sigma_z | l, m \rangle) && (2.141) \\ &= 2\hbar^2 |g|^2 \left(\langle l, m | \Sigma_+ \Sigma_-^{\text{corr}} | l, m \rangle + \tfrac{1}{2}N \right). && (2.142) \end{aligned}$$

2.6.7 Superradiance in master equation approach

Consider the *von Neumann* equation with dissipation

$$\frac{\partial \rho}{\partial t} = -\tfrac{i}{\hbar}[H_{JC}, \rho] + \tfrac{\kappa}{2}(2b\rho b^\dagger - \rho b^\dagger b - b^\dagger b \rho). \tag{2.143}$$

Equation (2.143) governs the density matrix of a light matter system described by the *Jaynes–Cummings* Hamiltonian with the cavity mode showing dissipation.

If κ is sufficiently large, it is possible to adiabatically eliminate the cavity mode, leading to the master equation (1),

$$\frac{\partial \rho_A}{\partial t} = \frac{2g^2}{\kappa}(2\Sigma_- \rho_A \Sigma_+ - \rho \Sigma_+ \Sigma_- - \Sigma_+ \Sigma_-), \tag{2.144}$$

where ρ_A is the density matrix of the atomic sub-system. Note that this corresponds formally to the dissipative term modeling emission into non-lasing modes introduced in chapter 2.4. The master equation approach has been adopted by previous work on superradiance ((14)). A comparison of the superradiant effects found for the full equation (2.143) and the master equation (2.144) is found in section 3.2.2).

Chapter 3

Numerical results

Numerical computations were carried out in Fortran90. The data pre– and post–processing was performed using Matlab 7.5. Computations were carried out on local computer clusters (Intel Quad Xeon processors).

In the first section results are presented for one and two atoms. These demonstrate basic properties of the theoretical model. In addition, since analytical results are available for a number of initial conditions the algorithmic accuracy can be established by first studying the one and two atom case.

In the second part, superradiant effects are presented in detail.

3.1 Numerical results for one and two atoms

In order to asses the reliability of the implemented algorithm and to gain a better insight into the physics of the model, in a first step numerical results will be compared to analytical solutions as far as the latter are available. First, the evolution of the atomic states in a pure *Jaynes-Cummings* system will be compared to the analytical result for one and two atoms. Second, the time evolution that is due to the *Lindblad* terms will be examined for each term separately. In a last step, both contributions are viewed together for the single atom case. Note that the choice of initial conditions is such that the algorithm can be checked. Once this is done more physical parameters are selected for the exploration of superradiance.

3.1.1 Pure Jaynes-Cummings dynamics

Single atom case

The Hamiltonian entering the *von-Neumann* equation for the density matrix is the pure *Jaynes-Cummings* Hamiltonian (2.37). We study a system with the photon field in the vacuum state and an excited atom with $\Omega = \omega$. The dynamics of the occupation probabilities are given by (2.51) for the excited state and (2.52) for the deexcited state with $n = 0$. We expect *Rabi* oscillations between both atomic states.

Figure 3.1 shows perfect agreement of the analytical and the numerical results. The same quality of agreement is obtained when there is a detuning between the field-mode and the atomic-transition energy.

Two atom case

The Hamiltonian entering the *von-Neumann* equation for the density matrix is now the two atom Hamiltonian (2.56) at resonance, i.e., $\Omega = \omega$. A comparison between numerical and analytical results for three different initial states will be subsequently discussed. The analytical results can be found in appendix B.

Full inversion

Figure 3.2 shows the comparison between the equations (2.1) to (2.4) and the numerical results. At $t = 0$ the state $|\alpha, \alpha, 0\rangle$ is occupied exclusively. Then its occupation probability drops in a manner comparable to the one atom case. Now a qualitatively new effect occurs. The probabilities for the three other states become non-zero, the states $|\alpha, \beta, 1\rangle$ and $|\beta, \alpha, 1\rangle$ showing identical dynamics. At an intermediate point, where $|\alpha, \alpha, 0\rangle$ and $|\beta, \beta, 2\rangle$ have equal occupation probabilities, the states $|\alpha, \beta, 1\rangle$ and $|\beta, \alpha, 1\rangle$ reach their maximum. One way of interpreting this is that to state $|\alpha, \alpha, 0\rangle$ relaxes via the states $|\alpha, \beta, 1\rangle$ and $|\beta, \alpha, 1\rangle$ to the atomic-system ground state. But the probability for $|\beta, \beta, 2\rangle$ never reaches 0. This can be understood by assuming that the occupation probability of $|\alpha, \beta, 1\rangle$ and $|\beta, \alpha, 1\rangle$ is not distributed entirely to the atomic ground state but an equal portion is returned to $|\alpha, \alpha, 0\rangle$ directly.

All atoms in lower state

Figure 3.3 shows the comparison between the equations (2.5) to (2.8) and the numerical results. The system dynamics show differences compared to the first case. The decay of the initial state is faster compared to scenario one. In both cases, the fully inverted state has a vanishing time-derivative at $t = 0$. In scenario one a change in this occupation number is required for any other changes due to trace conservation. This is not the case anymore now. The states $|\alpha, \beta, 1\rangle$ and $|\beta, \alpha, 1\rangle$ build up faster. Again, this can be viewed as the fully deexcited state being connected to the fully inverted state via the two intermediate states that first must have a non-zero occupation probability. As in the first scenario, the intermediate states decay into the fully inverted and deexcited state.

One atom excited

Figure 3.4 shows the comparison between the equations(2.9) to (2.12) and the numerical results. The system is initialized in the state $|\alpha, \beta, 1\rangle$ leading to identical dynamics compared to initial conditions set to $|\beta, \alpha, 1\rangle$. There is an oscillation between the occupation of the two states $|\alpha, \beta, 1\rangle$ and $|\beta, \alpha, 1\rangle$. Note the preference for the fully deexcited state.

3.1.2 Pure Lindblad dynamics

The analytical results for the *Lindblad* terms were derived in section 2.4.2 and their physical content discussed. Here, for a given choice of parameters a comparison between the exact results and the numerical dynamics is made. Note that for the pump-term and the emission into non-lasing modes only one sub-block of the density matrix corresponding to $n = 0$ was analyzed. This can be done since these two terms do not influence the photon field in any way, thus leading to identical dynamics for all values of n.

For the numerical evaluation of the cavity losses, a coherent field state was chosen, since the resulting dynamics can be obtained analytically, as seen in chapter 2.4.2. In addition, one numerical evaluation was performed with all off-diagonal terms set to one and the diagonal initialized with a poisson distribution . As expected, all matrix elements (but the ground

state) evolved towards zero. (With $\kappa = 1\frac{1}{ps}$ after $300\,ps$ the maximum matrix element - aside from the ground state - had a value of $6 \cdot 10^{-64}$; below the numerical accuracy of the computation .) As can be seen from figure 3.5 the dynamics of the occupation probabilities for the photonic states fall into three categories. First, the highest photon state (n=6) shows a monotonous decrease. Due to trace conservation, this must must lead to an increase for the lower states. This is observed. The second category is made up of all states besides the highest state (n=6) and the ground state. Here probability builds up, reaches a maximum and then decreases. The maximum occurs later for lower photon numbers. The third case is the dynamics of the ground state showing a monotonous increase asymptotically approaching unity.

Figures 3.6, 3.7 show the comparisons for pumping and emission into non-lasing modes. These processes are analogous in the sense that one can be converted to the other by swapping the excited and deexcited atomic state. This is reflected in the evolution of the occupation probabilities. While the excited state decays exponentially with the time constant (τ_{nl}) in the case of emission into non-lasing modes, the same is true for the ground state occupation probability in the case of pumping (decay rate P). In both cases the off-diagonal terms of the density matrix decay with $P/2$ and $2\tau_{nl}$, respectively.

3.1.3 Joint Jaynes-Cummings and Lindbald dynamics

For the dynamics of a system governed by both, the *Jaynes-Cummings* Hamiltonian and the *Lindblad* terms, no analytical results are available. But it is possible to make qualitative predictions and to test these numerically (see below). We will first consider cases in which only one *Landblad* term is present and finish the chapter by an analysis of the dynamics with all *Lindblad* terms present at once.

JC Hamiltonian with emission into non-lasing modes

Initializing the system with no photons in the resonator and an excited atom will lead to *Rabi* oscillations that decay exponentially due to emission into non-lasing modes. Indeed, this is observed as shown in figure 3.8. The time

constant of the decay is $\frac{1}{2\tau_{nl}}$, corresponding to the decay of the off-diagonal terms in the density matrix.

JC Hamiltonian with pumping

Pumping delivers energy to the system leading to a buildup of photons in the resonator. Therefore the pure *JC*-induces dynamics are altered due to the increase of photons in the cavity. This effect was suppressed in order to be able to check one process against the other. This was achieved by cutting the density matrix at $n_{Ph} = 1$ photons. The system was initialized with no photons in the resonator and the system deexcited. Pumping then leads to the same dynamics as emission into non-lasing modes, as can be seen from figure 3.9, with the excited and deexcited state interchanged.

JC Hamiltonian with cavity losses

The effect of additional cavity losses can be predicted from the effects of emission into non-lasing modes. Since there is an oscillatory exchange of photons and excitation between the atom and the field it should amount to the same result for the joint system if energy loss and elimination of off-diagonal terms occurs in the photonic or atomic part of the system. This is what is observed. When the same initial conditions are chosen as for cavity losses ($n_{Ph} = 0$ photons in the cavity and the atom in state $|\alpha\rangle$) the results shown in figure 3.10 are obtained.

JC Hamiltonian with all dissipative terms

Figure 3.11 shows the time evolution under the *Jaynes-Cummings* Hamiltonian and all three *Lindblad* terms. The system is initialized in the ground state ($|\beta, 0\rangle$).

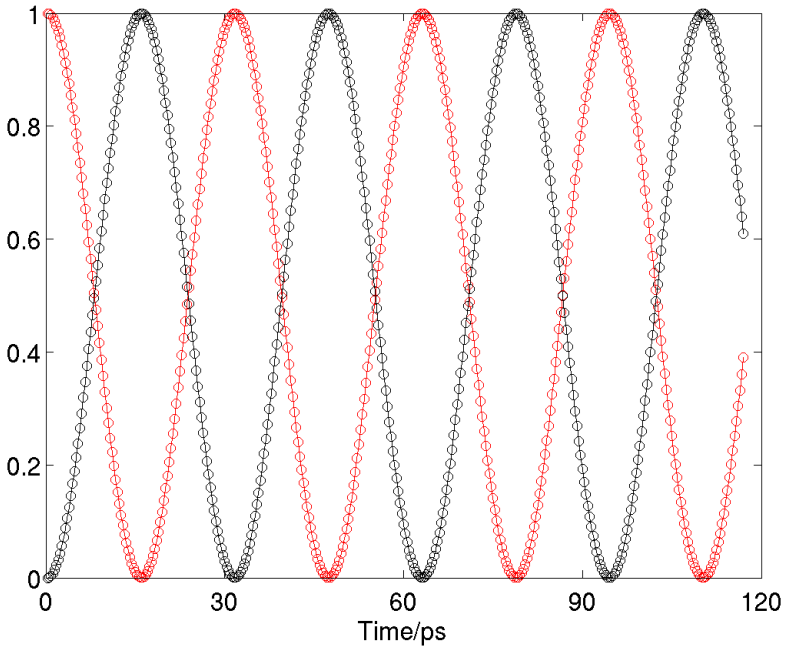

(a)

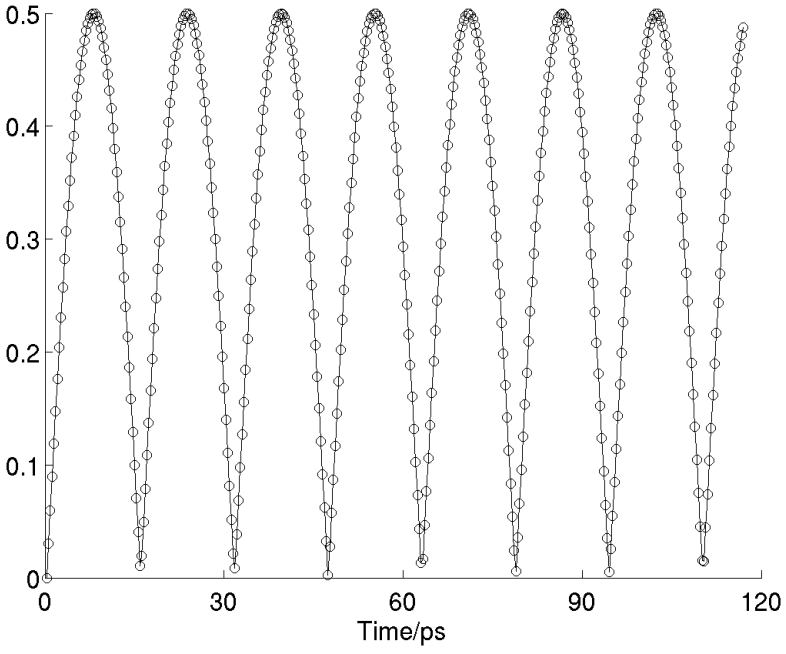

(b)

Figure 3.1: a) Comparison between the analytical dynamics (solid lines) and numerical results (crosses) for the occupation probabilities. The red color indicates the excited atomic state, the black color the deexcited state. The system is initialized at $n = 0$ photons, the coupling strength is $g = 0.1\,ps^{-1}$ and $\Omega = \omega$. b) Dynamics of the squared modulus of the transition amplitudes between the excited and deexcited state.

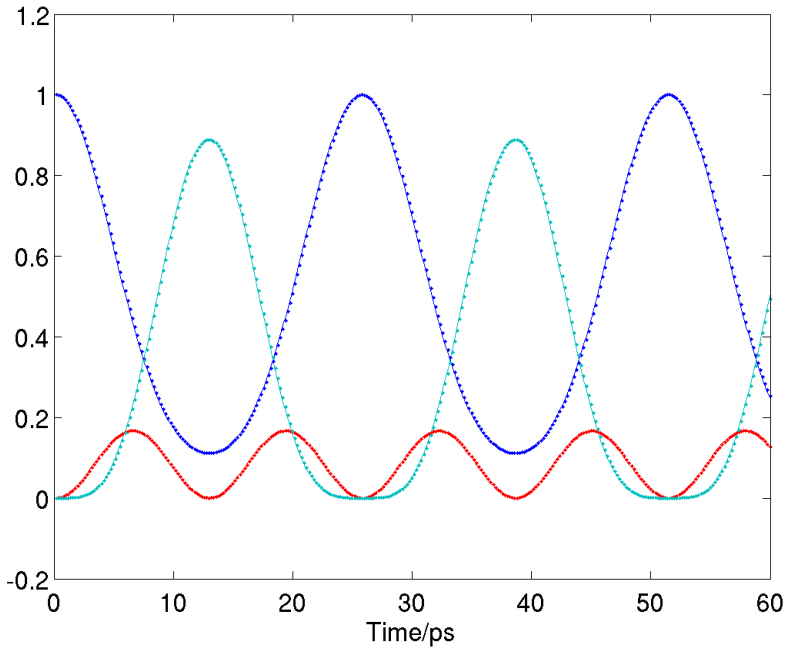

Figure 3.2: Comparison between the analytical dynamics (solid lines) and numerical results (dots) for the occupation probabilities. Blue corresponds to $|\alpha, \alpha, 0\rangle$, light green to $|\beta, \beta, 2\rangle$ and red the two other states. The system is initialized at $n = 0$ photons and full inversion. The coupling strength is $g = 0.1\,ps^{-1}$ and $\Omega = \omega$. The number of photonic states entering the computation is $N_P = 5$.

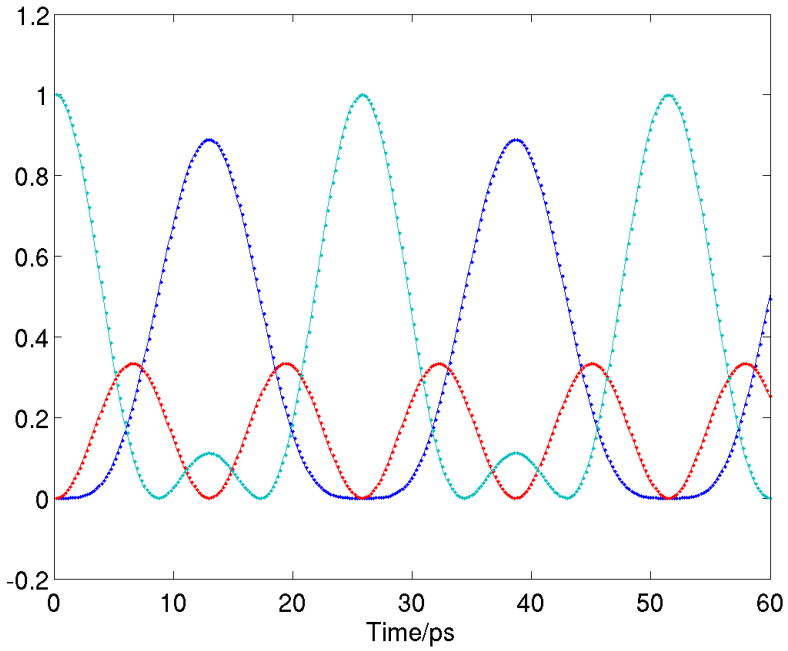

Figure 3.3: Comparison between the analytical dynamics (solid lines) and numerical results (dots) for the occupation probabilities. Blue corresponds to $|\alpha, \alpha, 0\rangle$, light green to $|\beta, \beta, 2\rangle$ and red the two other states. The system is initialized at $n = 2$ photons and all atoms deexcited. The coupling strength is $g = 0.1\,ps^{-1}$ and $\Omega = \omega$. The number of photonic states entering the computation is $N_P = 5$.

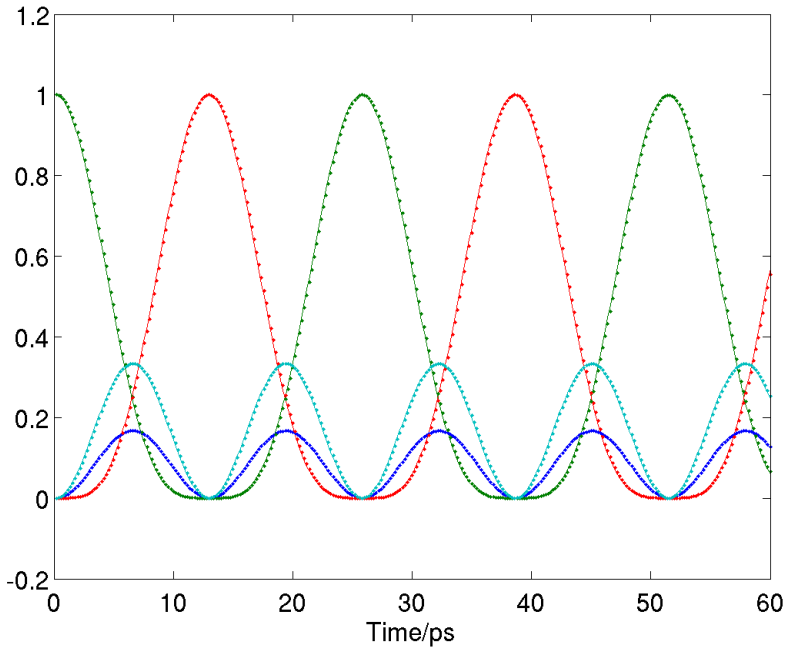

Figure 3.4: Comparison between the analytical dynamics (solid lines) and numerical results (dots) for the occupation probabilities. Blue corresponds to $|\alpha, \alpha, 0\rangle$, light green to $|\beta, \beta, 2\rangle$ and red and green the two other states. The system is initialized at $n = 1$ photons and one atom excited ($|\alpha, \beta, 1\rangle$). The coupling strength is $g = 0.1\, ps^{-1}$ and $\Omega = \omega$. The number of photonic states entering the computation is $N_P = 5$.

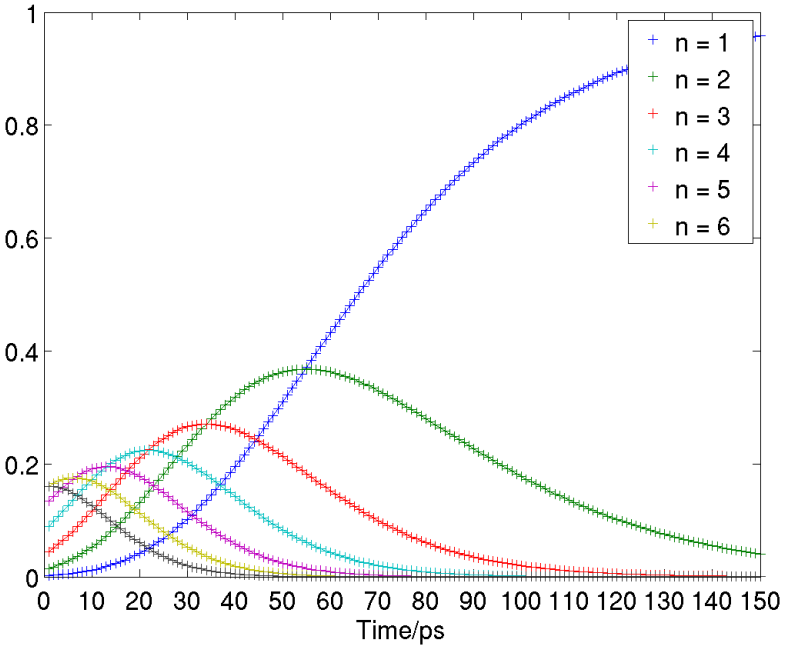

Figure 3.5: Analytical (solid lines) and numerical results (crosses) for the dynamics due to cavity losses. The density matrix was initialized with a poisson distributed photon-occupation number and all atoms in the excited state, all off-diagonal values were set to 0. The time evolution for $n = 0$ to $n = 6$ is shown. The parameter of the *Poisson* distribution is $\lambda = 6$, the cavity-loss rate $\kappa = 1/30\,ps^{-1}$.

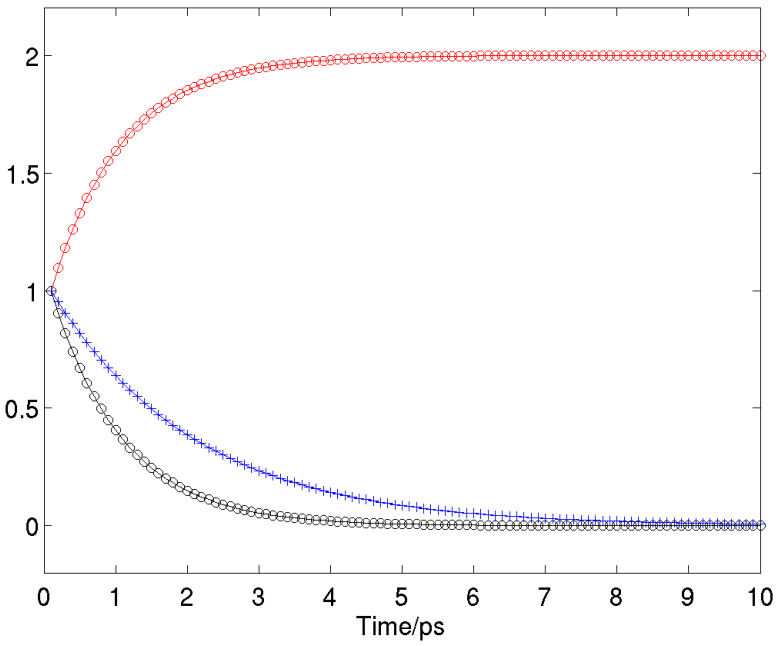

Figure 3.6: Comparison between the analytical (solid lines) and numerical results (crosses) for pump-induced dynamics. The red color indicates the excited atomic state, the blue color the deexcited state and the black color represents the squared modulus of the transition amplitudes. Only the part of the density matrix corresponding to $n = 0$ is taken into account, since dynamics are identical for other n. The (unphysical) initial condition of all entries equal to 1 was chosen, to make the relation of time constants transparent. The pump rate is $P = 1\frac{1}{ps}$.

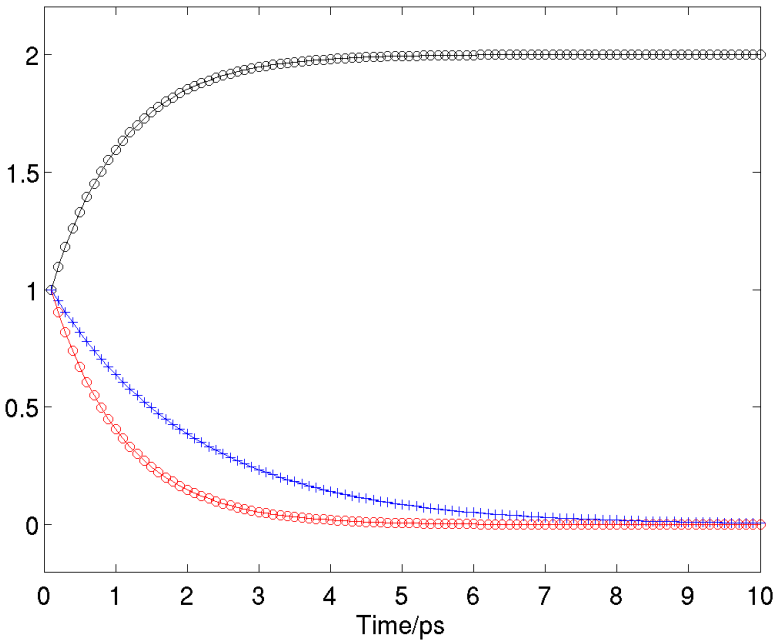

Figure 3.7: Comparison between the analytical (solid lines) and numerical results (crosses) for dynamics due to emission into non-lasing modes. The red color indicates the excited atomic state, the blue color the deexcited state and the black color represents the squared modulus of the transition amplitudes. Only the part of the density matrix corresponding to $n = 0$ is taken into account, since dynamics are identical for other n. The (unphysical) initial condition of all entries equal to 1 was chosen, to make the relation of time constants transparent. The pump rate is $\tau_{nl} = 1\,ps$.

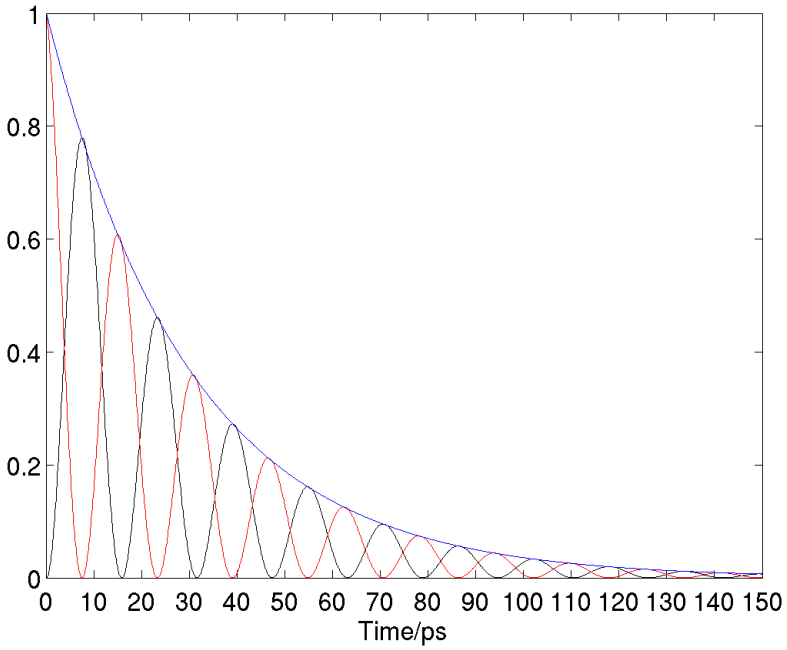

Figure 3.8: Numerical results for dynamics due to emission into non-lasing modes and the *JC* Hamiltonian. The red line indicates the occupation probability of the state $|\alpha>$, the black line is the expectancy value of the photon number, $<n>$. The system is initialized with an empty cavity and an excited atom. The coupling constant is $g = 0.2\, fs^{-1}$ and the emission parameter is $\tau_{nl} = 15\, fs$. The blue line is an exponential function: $e^{-\frac{1}{\tau_{nl}2}t}$

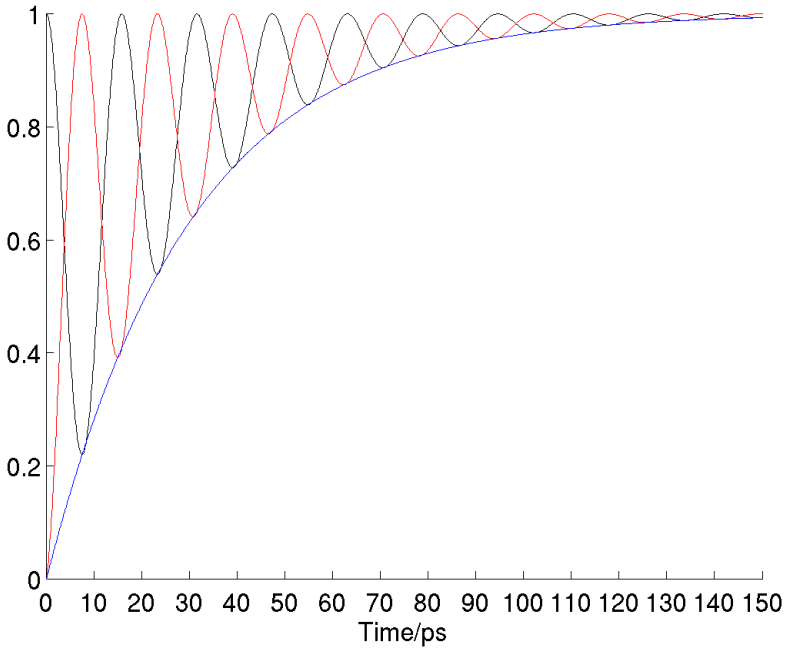

Figure 3.9: Numerical results for dynamics due to pumping and the *JC* Hamiltonian. The red line indicates the occupation probability of the state $|\alpha>$, the black line is the expectancy value of the photon number, $<n>$ in the cavity. The density matrix was cut at $n_{Ph} = 1$. The system is initialized with an empty cavity and a deexcited atom. The coupling constant is $g = 0.2\,ps^{-1}$ and the pump-rate is $P = \frac{1}{15}\,ps^{-1}$. The blue line is an exponential function: $e^{-\frac{P}{2}t}$ corresponding to the decay of the off-diagonal terms under pure *Lindblad* dynamics.

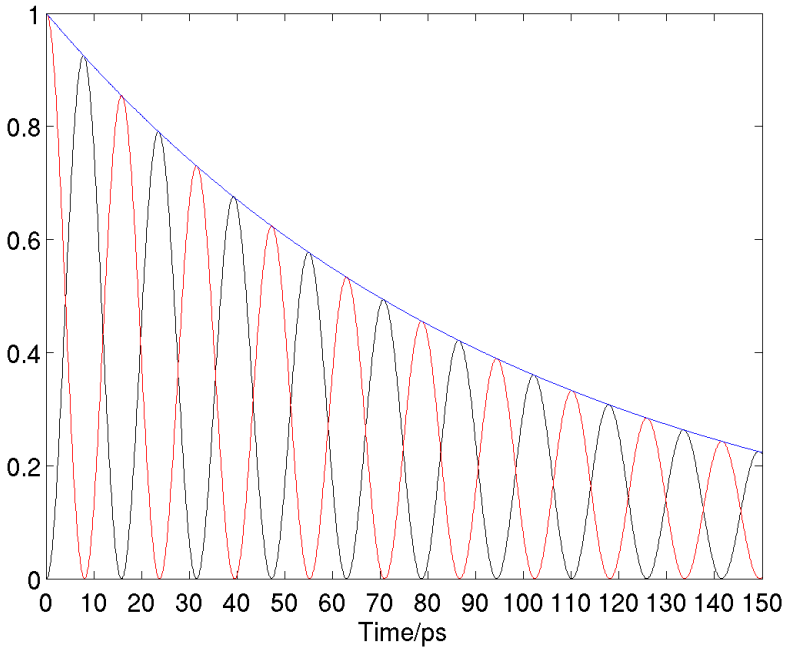

Figure 3.10: Numerical results for dynamics due to cavity losses and the *JC* Hamiltonian. The red line indicates the occupation probability of the state $|\alpha>$, the black line is the expectancy value of the photon number, $<n>$. The system is initialized with an empty cavity and an excited atom. The coupling constant is $g = 0.2\,ps^{-1}$ and the cavity constant is $\kappa = \frac{1}{50}\,ps^{-1}$. The blue line is an exponential function: $e^{-\frac{\kappa}{2}t}$ corresponding to the decay of the off-diagonal terms under pure *Lindblad* dynamics.

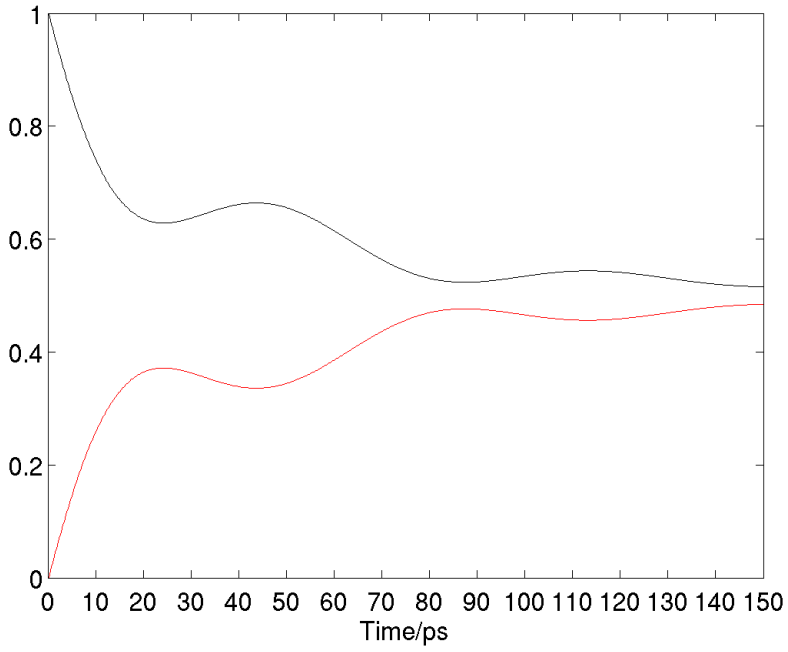

(a)

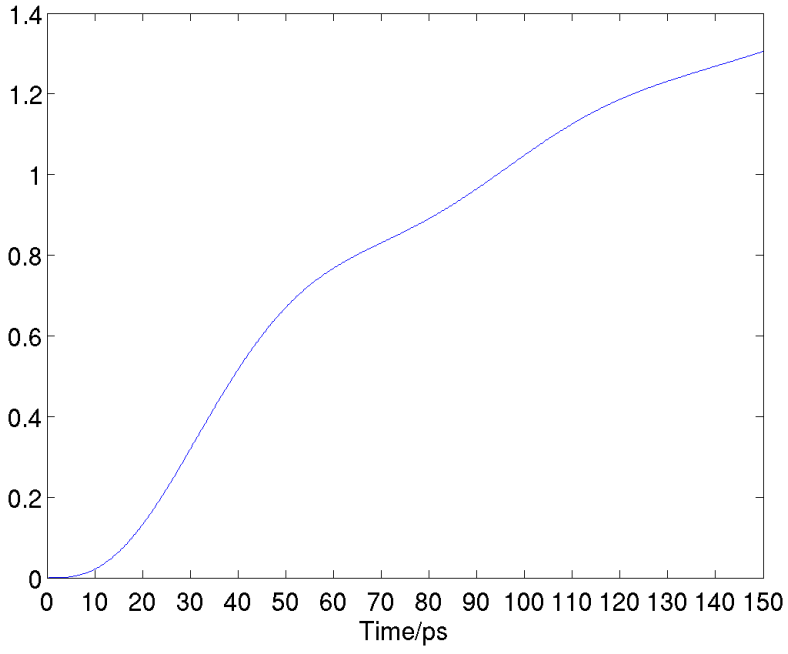

(b)

Figure 3.11: Occupation probabilities of the excited (red) and deexcited (black) state. b) Expectation value of the photon number $< n >$. Parameters are: $g = 0.1\, ps^{-1}$, $\kappa = \frac{1}{50}\, ps^{-1}$, $P = \frac{1}{15}\, ps^{-1}$, $\tau_{nl} = 1000\, fs$.

3.2 Numerical results for superradiant emission

3.2.1 Superradiant pulse from a fully inverted ensemble of N emitters

In figure (a) the (sign inverted) derivative of the energy of the atomic system is shown. A pronounced maximum, that scales quadratically with the number of emitters, is observed. Initially, the energy loss rate is simply N-times the single emitter case. Then coherence between the emitters is established. From a theoretical point of view this buildup of coherence can be understood as a consequence of the conservation of the eigenvalue of the Σ^2–operator. A reduction of the absolute value of $\langle \Sigma_z \rangle$ yields an increase in the sum of operator products measuring superradiant effects (see equation (2.102)). While the energy of the atomic system is decreased, the correlative part of the atomic polarization builds up. It reaches its maximum when the atomic system has already emitted half of its energy and then falls to zero again. The area under the curves in figure (a) must be proportional to the particle number due to energy conservation. The emission rate scales with an exponent always greater then one before and close to two when the maximum emission is reached. Therefore there must be a region after the maximum, where the emission of the N–emitters is less than N-times one emitter. This result is also observed.

3.2.2 Comparison between full dynamics an master equation approach

In section 2.6.7 the *von Neumann* equation of the *Jaynes–Cummings* Hamiltonian including cavity losses (2.143) is approximated by a master equation (2.144). The latter is formally identical with the dissipative term for emission into non-lasing modes. Therefore a comparison between the approximate and exact case can be made numerically within the model. Given that the parameter for cavity losses κ satisfies

$$\frac{|g|^2 N}{\kappa^2} << 1$$

the approximation is good (also known as the bad cavity limit,(1)). For many applications, e.g. lasers, cavities with very small values of κ are used. A

cavity with a quality factor of $Q = 10^4$ corresponds to a value of $\kappa = \frac{1}{40}\frac{1}{ps}$. Therefore the requirements of the approximation are not meet. In order to asses whether both calculations yield similar results, the parameters $g = 0.2\frac{1}{ps}$ and $\kappa = 1.5\frac{1}{ps}$ were chosen. The system is initialized at full inversion. The maximum number of emmitters is $N = 8$. This yields an intermediate value of

$$\frac{|g|^2 N}{\kappa^2} < 0.14.$$

The differences between the two cases can be seen in figure 3.12. The rate of energy loss of the atomic system is plotted against time. The energy rate is given in units of photons ($\Omega = \omega = 10^{15} Hz$) per ps, where ω is the atomic transition frequency and Ω the field mode frequency. The vanishing derivative for $t = 0$ for the full dynamics is typical for the *Jaynes–Cummings* system (see section 2.2.6). The master equation approach predicts emission rates at least half the maximum value for $t = 0$. In the bad cavity limit, the radiation is proportional to $\langle \Sigma_+ \Sigma_- \rangle$ (14):

$$I(t) = I_0 \hbar \omega \langle \Sigma_+ \Sigma_- \rangle.$$

This predicts a non-zero emission for $t = 0$, as observed.

Aside form the onset behavior, the emission–maxima show differences, as well. The delay observed in the exact case is a consequence of the explicit inclusion of the cavity mode. Since the buildup of coherence must be achieved by emission into and absorption out of the cavity mode, it is likely that the explicit inclusion introduces finite latency. An additional observation supports this hypothesis. The radiation shows a step increase for small t in both cases. For $t \leq 1\,ps$, the slope of the increase scales quadratically with the number of emitters in the approximate case, and linearly in the exact case. In both cases, it grows monotonously with the particle number. This linear scaling of the slope may be due to a lack of coherence in the exact case for small t.

Note that the maxima first occur later for higher atom numbers in the exact case. This trend is reversed for $N = 5$. This points towards a linear effect leading to a bigger latency that is then dominated by the quadratic superradiance more and more early in time. The pulse maxima scale quadratically with the number of emitters.

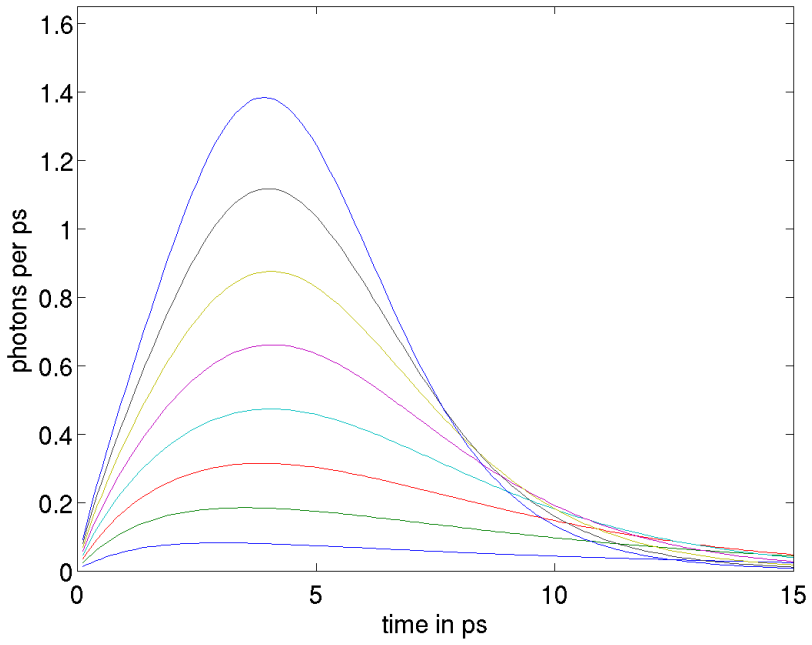

(a)

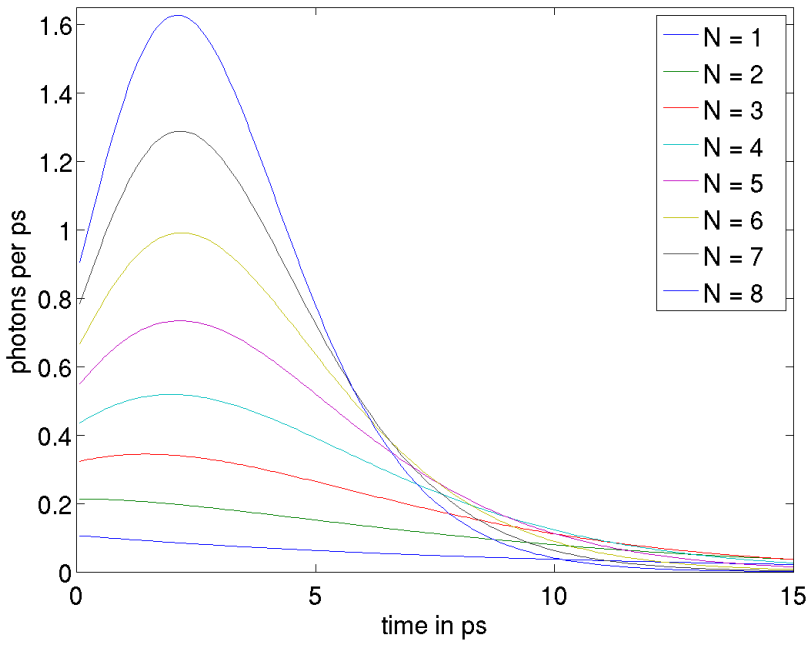

(b)

Figure 3.12: a) Temporal evolution of the radiation from $N = 1$ to $N = 8$ emitters. Jaynes–Cummings Hamiltonian with a coupling of $g = 0.2\frac{1}{ps}$ and cavity losses with $\kappa = 1.5\frac{1}{ps}$ included in calculation. Number of photonic states is $N_{ph} = 15$. b) Temporal evolution of the radiation from $N = 1$ to $N = 8$ emitters. Master equation corresponding to dynamics induced by only emission into non-lasing modes. $\tau_{nl} = \frac{\kappa}{|g|^2 N}$. See text for discussion.

3.2.3 Inhomogeneous Broadening

In currently available QD systems, emitters exhibit different resonance frequencies due to the manufacturing process. Numerical simulations were performed in order to predict the robustness of superradiant effects. While the effect of inhomogeneous broadening has been studied in the bad cavity limit (14), the present analysis is for a cavity–loss constant of $\kappa = 1.5\frac{1}{ps}$. This corresponds to the upper limit of a bad cavity regime. Three coupling strengths ($g = 0.05; 0.1; 0.2\frac{1}{ps}$) are combined with five different broadening magnitudes. Detunings are drawn from a Gaussian distribution with zero mean and FWHM $\Delta_i = 0.5; 1.0; 2.5; 5.0; 10meV$. They are in the order of detunings observed in real QDs. For quantification of superradiance in the presence of broadening, the parameter α is defined (14) as

$$\alpha^{-1} = \Delta_i \tau_{sr}, \qquad \tau_{sr} = \frac{\kappa^2}{2|g|^2 N}.$$

It tends to infinity for strict resonance. It is zero, if the FWHM is infinite. A value of $\alpha > 10$ corresponds to only negligable broadening. In the current evaluation, α values range from $\alpha = 0.52$ to $\alpha = 0.0167$ are used. For such values of α a strong decrease of coupling between emitters has been reported (14). For each combination of parameters 50 runs with $N = 5$ atoms are averaged.

The photon number expectation value $\langle n \rangle$ is shown in figure 3.13. Note that this quantity can not be computed in a master equation approach as (14); yet it is this quantity that may be measured in experiments. As can be seen from figure 3.13 the effect of inhomogeneous broadening is highly dependent on the detuning Δ. For the smallest coupling $g = 0.05\frac{1}{ps}$ and the greatest broadening $\Delta = 10meV$ the number of photons in the cavity is only 150% of the value observed for a *single* emitter. The emitters are detuned from the cavity mode thus emission is suppressed. As a consequence, almost no correlated atomic polarization is present. For a coupling four times larger ($g = 0.2\frac{1}{ps}$) the photon number is still only at ≈175% of the single emitter case. Keeping the coupling at a constant value $g = 0.05\frac{1}{ps}$ and reducing the detuning by a factor of 4 leads to a photon number of 350% of the single emitter case. Therefore the number of photons in the cavity is a non–linear function of the parameter α. The high sensitivity to detuning is a

consequence of the (comparably) low cavity losses. An exponential decay of cavity photons at a rate κ implies a loretzian energy distribution with a width in the order of $\approx 1.8meV$ (FWHM). The overlap between the this Loretzian and the distribution of atomic resonance frequencies will be a measure of the interaction of the atoms with the field mode. This overlap drops fast when detunings are in the same order as the FWHM of the energy distribution.

From figure 3.15 the time evolution of the atomic polarization $\langle \Sigma_+ \Sigma_- \rangle$ can be seen. For coupling strengths of $g = 0.1\frac{1}{ps}$ and $g = 0.2\frac{1}{ps}$ and low detuning, the bi-exponential decay reported by Tenmov (14) is reproduced. This is also observed for the mean photon number. This behavior results from the system transferring from a superradiant to a subradiant state (cf. figure 3.14). Such a transition is not possible in the resonant case, since the cooperation number (see section 2.6 for details) is conserved.

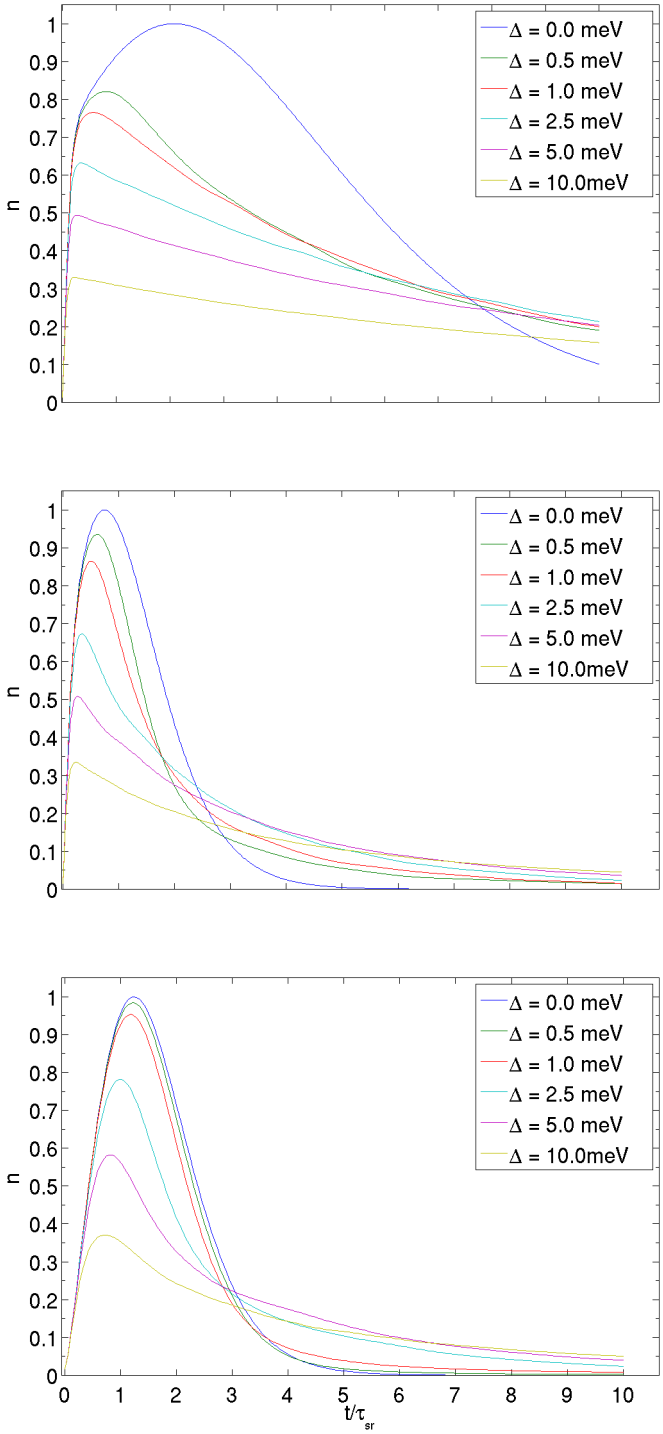

Figure 3.13: Inhomogeneous broadening: Normalized expectation value of photon number $\langle n \rangle / max(\langle n \rangle)$ for different detunings (see legend). Top: $g = 0.05\frac{1}{ps}$, middle: $g = 0.1\frac{1}{ps}$, bottom: $g = 0.2\frac{1}{ps}$. For all plots $\langle \omega \rangle = \Omega = 10^{15} Hz$ and $\kappa = 1.5\frac{1}{ps}$.

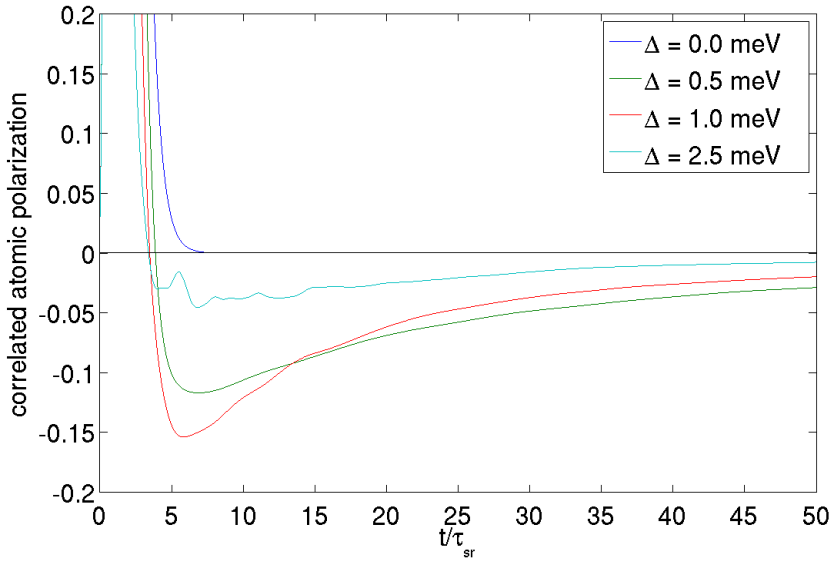

Figure 3.14: Inhomogeneous broadening: Expectation value of correlative atomic polarization $\langle \Sigma_+ \Sigma_- \rangle_{corr}$ for different detunings (see legend). Coupling strength $g = 0.2\frac{1}{ps}$, field mode frequency $\langle \omega \rangle = \Omega = 10^{15} Hz$ and cavity losses $\kappa = 1.5\frac{1}{ps}$. Positive values correspond to superradiant contributions to the emission process. As a consequence of the inhomogeneous broadening, transitions to subradiant states is observed.

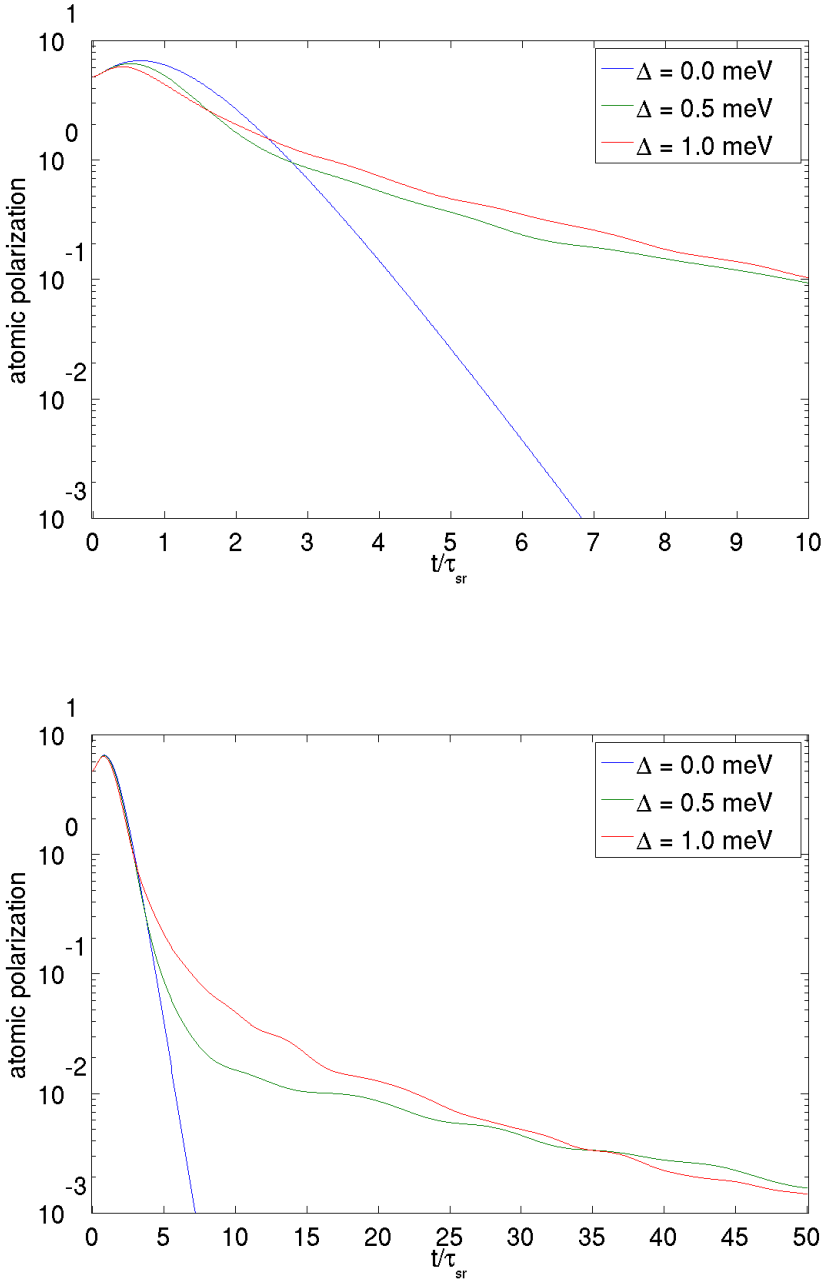

Figure 3.15: Inhomogeneous broadening: Expectation value of atomic polarization $\langle \Sigma_+ \Sigma_- \rangle$ for different detunings (see legend). Coupling strength $g = 0.1 \frac{1}{ps}$ (top) and $g = 0.2 \frac{1}{ps}$ (bottom), field mode frequency $\langle \omega \rangle = \Omega = 10^{15} Hz$ and cavity losses $\kappa = 1.5 \frac{1}{ps}$. The scale of the y-axis is logarithmic.

3.2.4 Suppression of superradiant emission

In the current model, superradiance is an interaction effect between a set of two–level systems. In order to separate contributions to emission from different sources, e.g., stimulated vs. spontaneous emission, one must find a way of manipulating both independently. In the theoretical treatment of superradiance (see section 2.6) the expectation value $\Sigma_+\Sigma_-$ was introduced as a measure of superradiance. The matrix elements of the density matrix ρ giving rise to this expectation value have the form

$$\langle \ldots, \alpha, \ldots \beta, \ldots | \rho | \ldots, \beta, \ldots \alpha, \ldots \rangle.$$

Suppression is achieved by setting these matrix elements to zero. A system of N emitters initialized at full inversion is then, to a good approximation, behaving like an N-fold copy of a single emitter. This can be seen from figure 3.16. The expectation value of the photon number $\langle n \rangle$ is plotted against time with suppression. In both plots the value for N-times the single atom case has been subtracted. If the N emitter system were merely the multiple of the single emitter system all lines should coincide. Differences are observed for the pulse maxima and the subsequent decay. With growing number of emitters there is an increasing overshot that is followed by a photon number that is smaller than expected. After $25ps$ this is reversed again and the N emitter systems show a larger photon number again. Note that while all maxima occur at the same time with suppression, there is a delay that increases for higher emitter numbers. What makes an interpretation of the data complicated is the interactions between photonic and atomic system (that are all not suppressed by the procedure) combined with the effects of cavity losses. Therefore only a qualitative discussion is possible. In an early phase of the pulse cavity losses are only very small since the loss rate is proportional to the photon number. This leads to a buildup of photons that is greater for many emitters. In addition, a greater photon number yields a higher intensity due to stimulated emission[1]. This explains the scaling of the observed maxima. The observed photon number then falls below the expected value at $t = 7.5\,ps$. This is $\approx 0.5\,ps$ after the atomic system is no longer inverted. Absorption processes that are again stronger in the many

[1] The matrix element $\langle n+1\, m-1 | \Sigma_- b^\dagger | n\, m \rangle$ is proportional to n, therefore transition probabilities are proportional to n in second order.

emitter case lead to a decrease in the photon number. The decay of photons in the cavity then becomes exponential with a different time constant for the emitters. This must be due to an interaction of cavity losses and the absorption and emission of the atomic system. In a rate approximation, the difference between absorption and emission must be shifted in favor of absorption for many emitters. This is the inverted case of the pulse onset. Note that the differences appear more pronounced for later times due to the logarithmic display. Turning to the case without suppression shown in figure 3.17, the temporal shift of maxima to later times for more emitters remains to be explained. This can be done by inspection of the correlated atomic polarization in figure 3.17. The correlation takes *longer* to build up for *few* emitters. For $N = 2$ it reaches its maximum at $5.8\,ps$. While the maximum for $N = 3$ emitters occurs only slightly earlier, it is larger by a factor of 3. Therefore it influences the emission process more. This shifts the maximum to a later time. For more emitters coherence builds up faster and the maximum shifts to earlier times for many emitters.

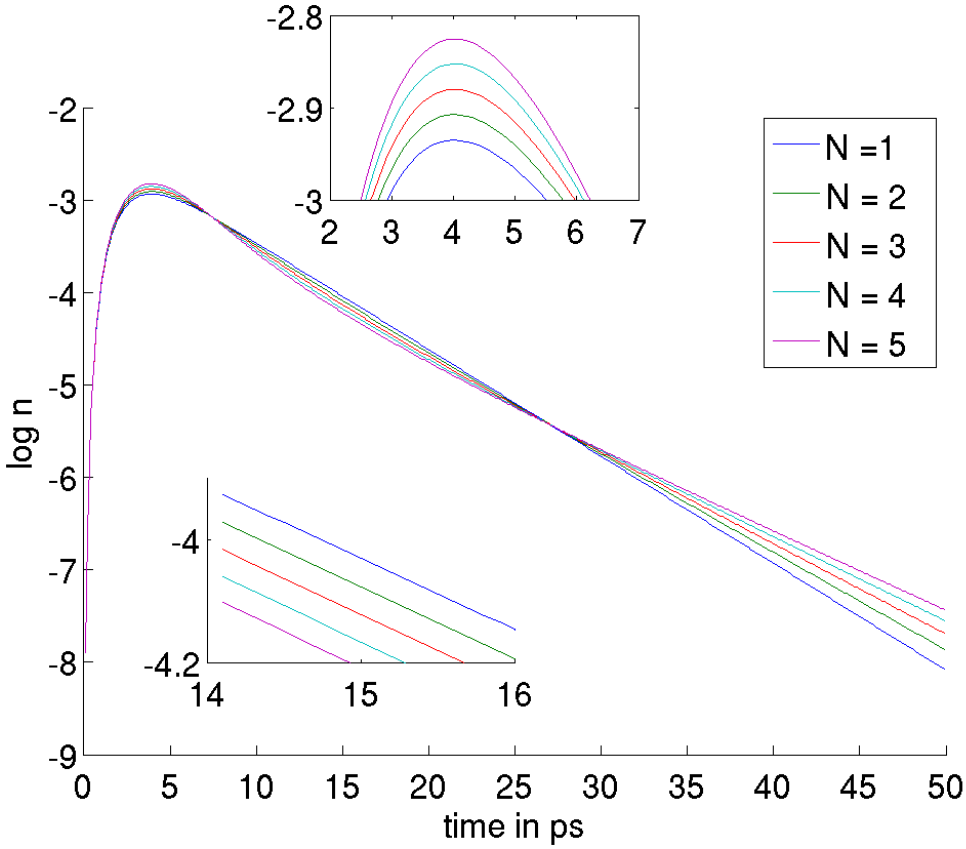

Figure 3.16: Suppression of superradiance: Normalized expectation value of cavity photon number $\langle n \rangle$ for different number of emitters (see legend). Coupling strength $g = 0.2\frac{1}{ps}$ and cavity losses $\kappa = 1.5\frac{1}{ps}$. Correlative elements of the density matrix are set to zero in every time step. The scale of the y-axis is logarithmic. The insets show an enlarged version of selected times.

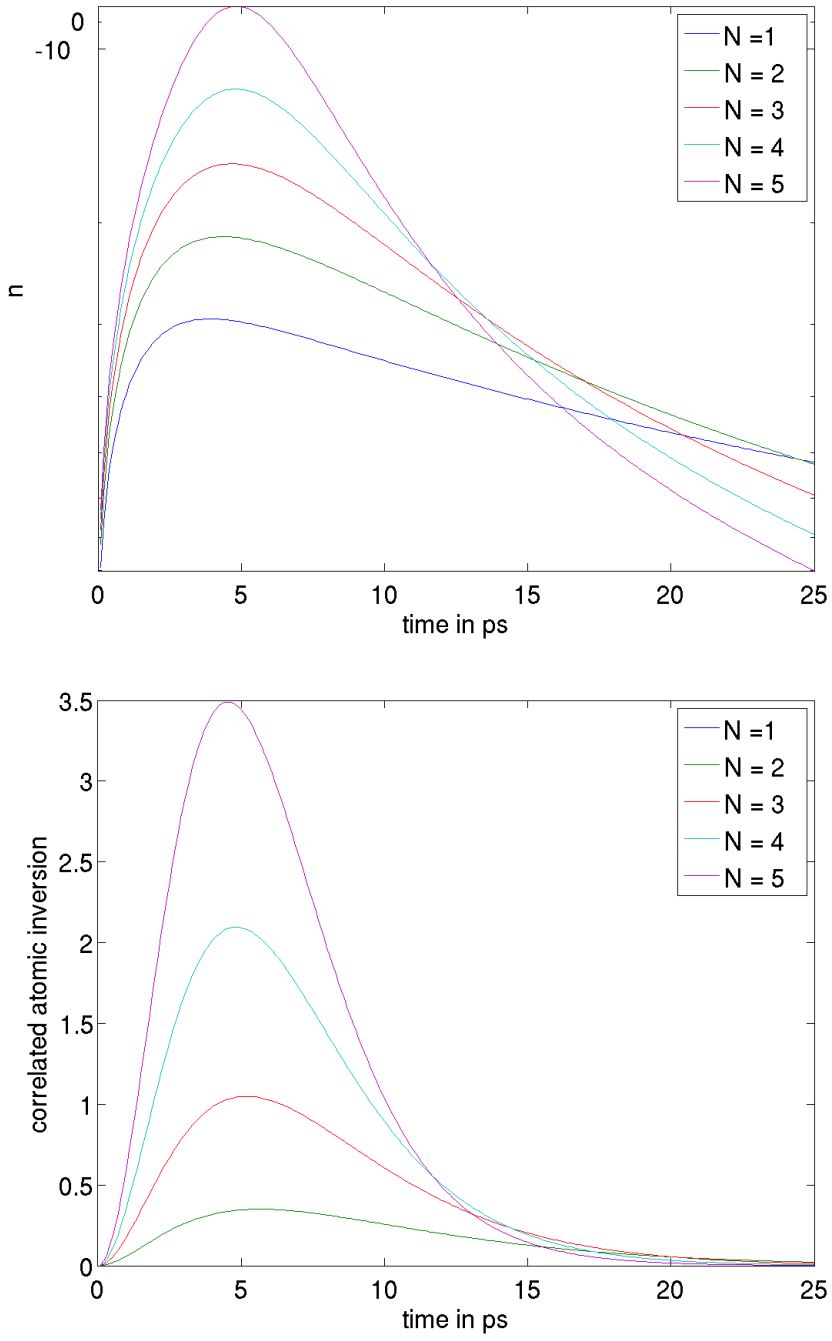

Figure 3.17: Suppression of superradiance. Top: Expectation value of cavity photon number $\langle n \rangle$ for different number of emitters (see legend). Coupling strength is $g = 0.2\frac{1}{ps}$ and cavity losses are $\kappa = 1.5\frac{1}{ps}$. Correlative elements of the density matrix are present. The scale of the y-axis is logarithmic.
Bottom: Correlated part of the atomic inversion.

Chapter 4

Summary and Outlook

A theoretical description of superradiance in the *Janyes–Cummings* framework was combined with numerical solution of the resulting *von Neumann* equation. Dissipation was included in *Born–Markov* approximation in the equations for the density matrix. A theoretical account of superradiance was given in a *Dicke* and product state basis. Both treatments were second order in the interaction (*Born* type). The predicted quadratic scaling of pulse maxima with number of emitters was observed in numerical simulation. The full solution of the problem was found to show differences from a master equation approach for cavity losses just below the bad cavity limit. The pulse onset was delayed and the maximum amplitude reduced in the exact case. Coherence between emitters proved sensitive to detuning. Results for $N = 5$ emitters showed a pronounced decrease in emission maxima for a weak coupling $g = 0.05\frac{1}{ps}$ when resonance frequencies show a broadening of $\Delta \approx 0.5meV$ (FWHM of a gaussian distribution, $\omega_0 = 10^{15}Hz$, cavity losses $\kappa = 1.5\frac{1}{ps}$). For stronger coupling ($g = 0.2\frac{1}{ps}$) pulse maxima are within 95% of the resonant case for detunings up to $\Delta = 1meV$. A bi-exponential is observed for these cases.

Subsequent work may be extended into several directions. First, a higher number of emitters may be included by implementation improvement, especially parallelization. Increasing the number of emitters may lead to an improved robustness of coherence in the presence of detuning. In addition, the implications of different parameter regimes on detuning–robustness may be analyzed. Beyond exploring sets of parameters in the the *Jaynes–Cummings*/*Born–Markov*–model, an enhancement in the theoretical description that include semiconductor effects, may provide a better understanding

of experimentally observed detuning–robustness.

Appendix A

Dissipation in Born Markov approximation

The *von-Neumann* equation in the interaction picture is

$$\frac{\partial \tilde{\rho}}{\partial t} = -\frac{i}{\hbar}[\tilde{H}_I(t), \tilde{\rho}(t)]. \tag{1.1}$$

The relation between an operator O and its interaction-picture description $\tilde{O}$ is

$$\tilde{O} = \exp(\tfrac{i}{\hbar}H_0\, t)\; O\; \exp(-\tfrac{i}{\hbar}H_0\, t). \tag{1.2}$$

We chose the interaction basis for further calculations since only the dynamics of the density matrix induced by the small interaction with the reservoir will give rise to the remaining dynamics.

We can formally integrate (1.1) to arrive at

$$\tilde{\rho}(t) = \tilde{\rho}(0) - \frac{i}{\hbar}\int_0^t [\tilde{H}_I(t'), \tilde{\rho}(t')]\; dt'. \tag{1.3}$$

Inserting (1.3) into (1.1) leads to

$$\frac{\partial \tilde{\rho}}{\partial t} = -\frac{i}{\hbar}[\tilde{H}_I(t), \tilde{\rho}(0)] - \hbar^{-2}\int_0^t [\tilde{H}_I(t), [\tilde{H}_I(t'), \tilde{\rho}(t')]]\; dt'. \tag{1.4}$$

We now assume that the initial density matrix factorizes $\rho(0) = \rho_S(0)R$, where ρ_S is the density matrix of the system. R is further assumed to be the equilibrium density matrix, i.e., $[R, H_R] = 0$ and remain in this state for all t: $R(t) = R(0)$, even when a system-bath interaction is present.

Making the factorization assumption for all times t is an approximation. Only terms at most 2nd order in H_I will enter the equation for ρ_S. For this reason the procedure is also referred to as *Born*-approximation. If H_I were zero, then $\dot{\tilde{\rho}}(t) = 0$; the dynamics of ρ will be fully controlled by H_S, since $[H_R, R] = 0$. In an expansion of ρ in H_I one gets in the *Schrödinger* picture:

$$\rho(t) = \rho_S(t)R(0) + O(H_I). \tag{1.5}$$

By inserting the expansion (1.5) into (1.4) one can show that any non-factorizing contributions will be at least 1st order in H_I and lead to 3rd order contributions. In order to keep the equation in 2nd order we must have factorization.

In a next step we take the trace over the bath contributions in (1.4):

$$tr_R\{\frac{\partial\tilde{\rho}}{\partial t}\} = \frac{\partial\tilde{\rho}_S}{\partial t} = -\frac{i}{\hbar}tr_R\{[\tilde{H}_I(t), \tilde{\rho}(0)]\} - \hbar^{-2}tr_R\{\int_0^t [\tilde{H}_I(t), [\tilde{H}_I(t'), \tilde{\rho}(t')]]\, dt'\}. \tag{1.6}$$

The first term on the RHS is:

$$\begin{aligned} tr_R\{[\tilde{H}_I(t), \tilde{\rho}(0)]\} &= tr_R\{[\tilde{H}_I(t), \rho_S(0)R]\} && (1.7)\\ &= tr_R\{\tilde{H}_I(t)\rho_S(0)R\} - tr_R\{\rho_S(0)R\tilde{H}_I(t)\} && (1.8)\\ &= tr_R\{\tilde{H}_I(t)R\}\rho_S(0) - \rho_S(0)\, tr_R\{R\tilde{H}_I(t)\} && (1.9)\\ &= [tr_R\{\tilde{H}_I(t)R\}, \rho_S(0)] && (1.10) \end{aligned}$$

The first step is possible since $\tilde{O}(0) = O$, the third because $[R, \rho_S] = 0$. In the last step the order of R and $\tilde{H}_I$ was switched. This is possible since R acts only on those degrees of freedom that are traced out.

In most cases $tr_R\{[H_I, R]\}$ is 0. If not, it can be made so by setting:

$$H = (H_0 + tr_R\{[H_I, R]\}) + (H_I - tr_R\{[H_I, R]\}) = H_0' + H_I'.$$

We specify the interaction to have the form:

$$H_I = \sum_\alpha [\hbar g_\alpha \hat{s}_\alpha^\dagger \hat{\Gamma}_\alpha + \hbar g_\alpha^* \hat{s}_\alpha \hat{\Gamma}_\alpha^\dagger] := \hbar \sum_\alpha s_\alpha \Gamma_\alpha$$

s_α denotes a system and Γ_α a bath operator. We include the hermitian conjugate to ensure the hermiticty of H_I. In the last term this inclusion is only

implicit. This makes the following calculations more handy:

$$\frac{\partial \tilde{\rho}_S}{\partial t}(t) = -\int_0^t tr_R \left\{ [\sum_\alpha \tilde{s}_\alpha(t)\tilde{\Gamma}_\alpha(t), [\sum_\beta \tilde{s}_\beta(t')\tilde{\Gamma}_\beta(t'), \tilde{\rho}_S(t')R]] \right\} dt' \quad (1.11)$$

$$= -\sum_{\alpha,\beta} \int_0^t [\tilde{s}_\alpha(t)\tilde{s}_\beta(t')\tilde{\rho}_S(t')\ tr_R\{\tilde{\Gamma}_\alpha(t)\tilde{\Gamma}_\beta(t')R\} + \cdots\ dt' \quad (1.12)$$

$$= -\sum_{\alpha,\beta} \int_0^t (\tilde{s}_\alpha(t)\tilde{s}_\beta(t')\tilde{\rho}_S(t') - \tilde{s}_\beta(t')\tilde{\rho}_S(t')\tilde{s}_\alpha(t))\langle\tilde{\Gamma}_\alpha(t)\tilde{\Gamma}_\beta(t')\rangle_R dt' \quad (1.13)$$

$$-\sum_{\alpha,\beta} \int_0^t (\tilde{\rho}_S(t')\tilde{s}_\beta(t')\tilde{s}_\alpha(t) - \tilde{s}_\alpha(t)\tilde{\rho}_S(t')\tilde{s}_\beta(t'))\langle\tilde{\Gamma}_\beta(t')\tilde{\Gamma}_\alpha(t)\rangle_R dt' \quad (1.14)$$

In a next step we will make two additional simplifications. First, we assert that the interaction–picture induced time dependence of the sytstem operators is an oscillation; i.e., that the equation

$$\tilde{s}_j(t') = \tilde{s}_j(t)\, e^{i\varepsilon_j(t-t')}$$

holds.

This makes it possible to pull the system operators in front of the integral, leaving inside only an exponential factor oscillating at one of the systems eigenfrequencies. In some cases this is only an approximation [1].

Second, we invoke the *Markov* approximation which states that we can replace $\tilde{\rho}_S(t')$ by $\tilde{\rho}_S(t)$ and set the lower bound of the integration to $-\infty$. The equation (1.11) for the density matrix now reads:

[1] In fact this is true already for a *Jaynes-Cummings* Hamiltonian. As an example we take the atomic raising operator σ_+. It's *Heisenberg* equation is:

$$\frac{\partial \sigma_+}{\partial t} = i(\hbar\omega\sigma_+ - \hbar 2gb\sigma_z).$$

The time evolution of the σ-operators is coupled. This lo longer leads to a solution $\sigma_+(t) = \sigma_+(0)\exp(i\hbar\omega)$. The deviation from the assumed case is more severe, when the coupling constant g is increased. One may argue that as long g is small enough the oscillatory case is a good approximation.

$$\frac{\partial \tilde{\rho_S}}{\partial t}(t) = -\sum_{\alpha,\beta}(\tilde{s}_\alpha(t)\tilde{s}_\beta(t)\tilde{\rho_S}(t) - \tilde{s}_\beta(t)\tilde{\rho_S}(t)\tilde{s}_\alpha(t)) \tag{1.15}$$

$$\int_{-\infty}^{t} e^{i\varepsilon_\beta(t-t')}\langle\tilde{\Gamma}_\alpha(t)\tilde{\Gamma}_\beta(t')\rangle_R dt' \tag{1.16}$$

$$-\sum_{\alpha,\beta}(\tilde{\rho_S}(t')\tilde{s}_\beta(t)\tilde{s}_\alpha(t) - \tilde{s}_\alpha(t)\tilde{\rho_S}(t)\tilde{s}_\beta(t)) \tag{1.17}$$

$$\int_{-\infty}^{t} e^{i\varepsilon_\beta(t-t')}\langle\tilde{\Gamma}_\beta(t')\tilde{\Gamma}_\alpha(t)\rangle_R dt' \tag{1.18}$$

In order to proceed we must specify the Hamiltonian of the bath. We select the bath Hamiltonian to be a set of harmonic oscillators (omitting the ground state energy):

$$H_R = \sum_n E_n B_n^\dagger B_n \tag{1.19}$$

The strength with which each mode is coupled to the system will be, in general, different for each mode. The relation between the operators Γ_i that couple the system to the bath and the operators B and $B^\dagger$ in the bath Hamiltonian (1.19) therefore are:

$$\Gamma_\alpha = \sum_n \kappa_{n,\alpha} B.$$

With this type of thermal bath, the differential equation (1.18) for $\tilde{\rho}_S$ can be further simplified (see Chapter 1.4 in (4)) .

In this case we finally have:

$$\frac{\partial \tilde{\rho_S}}{\partial t}(t) = \sum_\alpha \frac{\kappa_\alpha}{2}(2\tilde{s}_\alpha(t)\tilde{\rho_S}(t)\tilde{s}_\alpha^\dagger(t) - \tilde{\rho_S}(t)\tilde{s}_\alpha^\dagger(t)\tilde{s}_\alpha(t) - \tilde{s}_\alpha^\dagger(t)\tilde{s}_\alpha(t)\tilde{\rho_S}(t)) \tag{1.20}$$

which reads

$$\frac{\partial \rho_S}{\partial t} = -\frac{i}{\hbar}[H_S, \rho_S] + \sum_\alpha \frac{\kappa_\alpha}{2}(2s_\alpha\rho_S s_\alpha^\dagger - \rho_S s_\alpha^\dagger s_\alpha - s_\alpha^\dagger s_\alpha \rho_S) \tag{1.21}$$

in the *Schrödinger* picture.

Appendix B

Solutions for the two atom JC Hamiltonain for three initial conditions

Solving the Hamiltonian (2.56) yields the occupation probabilities $|C_j(t)|^2$. For three different initial conditions the analytical results are presented. The comparison with numerical results is found in section 3.1.

We first chose the system to be initialized at full inversion with no photons in the cavity, i.e., $C_{\alpha,\alpha,0}(0) = 1$. For the $|C_j|^2$ the results are

$$|C_{\alpha,\alpha,0}|^2(t) = \frac{(2+\cos(g\sqrt{6})t)^2}{9}, \tag{2.1}$$

$$|C_{\alpha,\beta,0}|^2(t) = \frac{\sin^2(g\sqrt{6}\,t)}{6}, \tag{2.2}$$

$$|C_{\beta,\alpha,0}|^2(t) = \frac{\sin^2(g\sqrt{6}\,t)}{6}, \tag{2.3}$$

$$|C_{\beta,\beta,0}|^2(t) = \frac{8\sin^4(g\sqrt{6}/2\cdot t)}{9}. \tag{2.4}$$

We next chose the system to be initialized with all atoms deexcited and

2 photons in the cavity, i.e., $C_{\beta,\beta,2}(0) = 1$. For the $|C_j|^2$ the results are

$$|C_{\alpha,\alpha,2}|^2(t) = \frac{(1 + 2\cos(g\sqrt{6})t)^2}{9}, \tag{2.5}$$

$$|C_{\alpha,\beta,2}|^2(t) = \frac{2\sin^2(g\sqrt{6}\,t)}{6}, \tag{2.6}$$

$$|C_{\beta,\alpha,2}|^2(t) = \frac{2\sin^2(g\sqrt{6}\,t)}{6}, \tag{2.7}$$

$$|C_{\beta,\beta,2}|^2(t) = \frac{4\cdot 2\sin^4(g\sqrt{6}/2\cdot t)}{9}. \tag{2.8}$$

Finally, we chose the system to be initialized at $C_{\alpha,\beta,1}(0) = 1$. For the $|C_j|^2$ the results are

$$|C_{\alpha,\alpha,2}|^2(t) = \frac{\sin^2(g\sqrt{6}\,t)}{6}, \tag{2.9}$$

$$|C_{\alpha,\beta,2}|^2(t) = \cos^4(g\sqrt{6}\,t), \tag{2.10}$$

$$|C_{\beta,\alpha,2}|^2(t) = \sin^4(g\sqrt{6}\,t), \tag{2.11}$$

$$|C_{\beta,\beta,2}|^2(t) = \frac{2\sin^2(g\sqrt{6}\,t)}{6}. \tag{2.12}$$

A comparison with numerical data can be found in section (3.1.1).

Appendix C

Commutation Relations of Σ-Operators

The operators of total *spin* Σ_i for N single *spin* operators σ_i are defined as

$$\Sigma_x = \sum_i = 1^N \sigma_x, \tag{3.1}$$

$$\Sigma_y = \sum_i = 1^N \sigma_y, \tag{3.2}$$

$$\Sigma_z = \sum_i = 1^N \sigma_z. \tag{3.3}$$

Note that when the operators are used to describe the atomic two-level system they are dimensionless. They satisfy the commutation relation

$$[\Sigma_i, \Sigma_j] = i\,\varepsilon_{ijk}\Sigma_k, \quad (i, j, k = x, y, z). \tag{3.4}$$

By linear combination of the above operators, the raising operator Σ_+ and its adjoint, the lowering operator, can be written as

$$\Sigma_+ = \Sigma_x + i\Sigma_y, \tag{3.5}$$

$$\Sigma_+ = \Sigma_x - i\Sigma_y. \tag{3.6}$$

$$\tag{3.7}$$

The operator of the squared total *spin* is defined as

$$\Sigma^2 = \Sigma_x^2 + \Sigma_y^2 + \Sigma_z^2. \tag{3.8}$$

This may be rewritten as

$$\Sigma^2 = \Sigma_z^2 + \tfrac{1}{2}(\Sigma_+\Sigma_- + \Sigma_-\Sigma_+). \tag{3.9}$$

The commutation relations for Σ^2 and $\Sigma_\pm$ are

$$[\Sigma_+, \Sigma_-] = 2\Sigma_z \tag{3.10}$$

$$[\Sigma_z, \Sigma_\pm] = \pm \Sigma_\pm \tag{3.11}$$

$$[\Sigma^2, \Sigma_i] = 0. \tag{3.12}$$

$$\tag{3.13}$$

The operator Σ^2 commutes with all the other Σ operators. This makes its eigenvalues conserved quantities if the Hamiltonian contains only Σ_i operators.

Bibliography

[1] G. S. Agrawal. Master-equation approach to spontaneous emission. iii. many-body aspects of emission from two-level atoms and the effect of inhomogeneous broadening. *Phys. Rev. A*, 4:1791, 1971. [6, 44, 61]

[2] L. Allen and J.H. Eberly. *Optical Resonance and Two-Level Atoms*. Interscience monographs and texts in physics and astronomy, v. 28. Wiley-Interscience, 1975. [8]

[3] M. Lorke C. Gies, J. Wiersig and F. Jahnke. Semiconductor model for quantum-dot-based microcavity lasers. *Phys. Rev. B*, 75:0138031–1–1, 2007. [5]

[4] H.J. Carmichael. *Statistical Methods in Quantum Optics 1*. Springer, 1999. [78]

[5] R. H. Dicke. Coherence in spontaneous radiation processes. *Phys. Rev.*, 93(1):99, Jan 1954. [6, 33, 37]

[6] J.N. Franklin. *Matrix Theory*. Series in Applied Mathematics. Prentice-Hall, 1968. [29]

[7] Roy J. Glauber. The quantum theory of optical coherence. *Phys. Rev.*, 130(6):2529–2539, Jun 1963. [12]

[8] John David Jackson. *Classical Electrodynamics*. Wiley, 1998. [13]

[9] E. T. Jaynes and F. W. Cummings. Comparison of quantum and semiclassical radiation theories with application to the beam maser. *Proceedings of the IEEE*, 51(1):89–109, 1963. [8]

[10] L. Mandel and E. Wolf. *Optical coherence and quantum optics*. Cambridge University Press, 1995. [38, 39, 41]

[11] P. Meystre and M. Sargent III. *Elements of Quantum Optics*. Springer, 3rd edition edition, 1999. [9, 18]

[12] A. Rogach. *Semiconductor Nanocrystal Quantum Dots: Synthesis, Assembly, Spectroscopy and Applications*. Springer, 2008. [5]

[13] L. I. Schiff. *Quantum mechanics*. McGraw-Hill, Inc., 1968. [11, 13]

[14] V. Temnov and U. Woggon. Superradiance and subradiance in an inhomogeneously broadened ensemble of two-level systems coupled to a low-q cavity. *Rhys. Rev. Lett.*, 95:243602, 2005. [6, 7, 34, 42, 44, 62, 64, 65]

[15] N. Lendentsov V. Shchukin and D. Bimberg. *Epitaxy of Nanostructures (Nanoscience and Technology)*. Springer, 2003. [5]

[16] J. Venables. *Introduction to Surface and Thin Film Processes*. Cambridge University Press, 2000. [5]